Computational studies of experimentally observed structures of sulfur on metal surfaces

Dominic R. Alfonso

National Energy Technology Laboratory, U. S. Department of Energy,
Pittsburgh, PA 15236

Abstract

First-principles electronic structure calculations were carried out to examine the experimentally observed structures of sulfur on close packed surfaces of a number of important metals - Ag(111), Cu(111), Ni(111), Pt(111), Rh(111), Re(0001) and Ru(0001). At low coverages ($\leq \frac{1}{3}$ ML), the prediction is consistent with the typical pattern of preferred sulfur occupancy of threefold hollow sites, notably the fcc site on the (111) surfaces and the hcp site on the (0001) surfaces. Theoretical confirmation for the existence of pure sulfur overlayer phases on Pt(111), Rh(111), Re(0001) and Ru(0001) at higher coverages ($> \frac{1}{3}$ ML) was provided. For the ($\sqrt{7} \times \sqrt{7}$) phase seen on Ag(111), the most preferred structure identified for adsorbed S trimer consists of an S atom on the top site bonded to two S atoms situated on the nearest neighbor off-bridge site positions. Among the different densely packed mixed sulfur-metal overlayer models suggested for the ($\sqrt{7} \times \sqrt{7}$) phase on Cu(111), the structure which consists of metal and S atoms in a hexagonal-like arrangement on the top substrate was found to be the most energetically favorable. For the ($5\sqrt{3} \times 2$) phase on Ni(111), the calculations confirm the existence of clock-reconstructed top layer metal atoms onto which sulfur atoms are adsorbed.

1. Introduction

It is a well known fact that the presence of adsorbed sulfur has a deleterious impact on the surface reactivity of metals. A range of chemistries including methanation, alkane hydrogenolysis, olefin hydrogenation and water-gas shift reactions are adversely affected. [1-5] Sulfur poisoning is also a major issue in metal based membranes used in coal gasification, where high enough dissociation rates for the H_2 must be maintained for optimal performance.[6,7]

A detailed knowledge of S interaction with metals needs to be obtained in order to understand such effects. S interaction with metals has been intensively investigated and much of the previous work focused largely on the experimental studies of surface structure. It is known that S atoms form a rich range of structures on close-packed surfaces of several important noble and transition metals - Ag(111) [8-11], Cu(111) [12-17], Ni(111) [18-27], Pt(111) [28-31], Rh(111) [32-35], Re(0001) [36-39] and Ru(0001) [40-44]. On Ni(111), Pt(111), Re(0001) and Ru(0001), S exhibit a (2 × 2) phase at coverage θ_S= ¼ ML. The ($\sqrt{3} \times \sqrt{3}$) phase is seen on Ag(111), Ni(111), Pt(111), Rh(111) and Ru(0001) at θ_S= ⅓ ML while Re(0001) has a c($\sqrt{3} \times 5$) phase detected at θ_S= ⅕ ML. These low coverage phases were determined to consist of S overlayer with one adsorbate per unit mesh on an essentially undistorted metal substrate. The general trend is toward the adsorbates occupying high symmetry three-fold adsorption sites, notably the fcc hollow site on the (111) surface and the hcp hollow site on the (0001) surface.

The phases observed at high coverages are found to be quite varied and more complex. With increasing coverage (or post-annealing to above room temperatures), formation of phases with either pure S overlayer or mixed overlayer structure was found. On Ag(111), a ($\sqrt{7} \times \sqrt{7}$) phase was observed after exposure to sulfur containing compound such as H_2S

using scanning tunneling microscopy (STM).[10] This phase was also detected with low-energy electron diffraction (LEED) after subjecting the Ag(111) from oxidative underpotential deposition of sulfur [11], H_2S gas dosing above 10^{-3} torr at temperatures up to 673 K, [9] and S_2 dosing at 300 K [8]. A number of conflicting models based on S overlayer structure with $\theta_S = 3/7$ ML were proposed. Just as was the case for Ag(111), the ($\sqrt{7} \times \sqrt{7}$) is also the widely observed phase formed by S on Cu(111) at high coverage.[12-17] The low coverage ($\sqrt{3} \times \sqrt{3}$) phase on Cu(111) was reported in a very early work [12] but its existence has not been reproduced in any subsequent studies. Data from LEED, surface extended X-ray absorption fine structure (SEXAFS), normal incidence X-ray standing wave (NIXSW) and surface X-ray diffraction (SXRD) analyses suggest that the structure of the ($\sqrt{7} \times \sqrt{7}$) phase is not a simple S overlayer. It is more consistent with models which consist of mixed S-Cu structure with $\theta_S = 3/7$ ML. However, the various models proposed have apparent disagreement in terms of geometrical details. The model proposed, for example, by Domangue and Oudar and supported by later experiments of Prince *et al*. consists of Cu and S atoms in a hexagonal-like arrangement on the top substrate layer.[12,13] By contrast, the model proposed by Foss *et al.* [15] consists of four in-plane Cu per unit mesh on the top layer. One S atom sits above and bonded to these metal atoms forming a Cu_4S fragment. Additionally, two S atoms are buried underneath this fragment. This picture was favored in subsequent studies [17,45] but was rejected by Saidy and Mitchell [16] who suggested a modified version of the model proposed by Domangue and Oudar.

While the ($\sqrt{7} \times \sqrt{7}$) LEED pattern is typically seen on Ag(111) and Cu(111), a variety of structures is observed at higher coverages depending on the metal substrate. For example, the ($5\sqrt{3} \times 2$) phase is seen on Ni(111) at high coverage. This phase has attracted significant interest with early studies indicating that it consists of a reconstructed top Ni

layer containing sixteen metal atoms per unit mesh (θ_{Ni}= ⅘ ML). It is similar to a single layer of Ni(100), onto which eight S atoms are chemisorbed (θ_S= ⅖ ML).[24-27] A clock-reconstructed version of this model was proposed in subsequent studies. In this model, the top metal overlayer consists of pairs of square-like tetramers rotated alternately, clockwise and anti-clockwise, with S atoms exhibiting a (2 × 2) periodicity with respect to the metal overlayer.[23,46,47] In the case of Pt(111), early LEED investigations identified a (7 × √ 3) phase at θ_S= ⅜ ML.[28] Subsequent studies proposed a pure S overlayer model where two S are on the fcc sites and one on the hcp site per unit cell. LEED pattern associated with (7 × √ 3) was also found on Rh(111) with S occupancy suggested to be similar to that in Pt(111).[34,35] Additionally, S forms other phases on Rh(111) with c(4 × 2), (4 × 4) and (7 × 7) periodicity at θ_S > 3/7 ML.[33-35] The coverage of both c(4 × 2) and (4 × 4) phases were determined to be θ_S= ½ ML and it was suggested that in the former, the fcc and hcp sites are equally occupied by S while in the latter case, they are adsorbed exclusively on the fcc site. On Re(0001), S forms distorted trimers, tetramers and hexamers arranged in (3√ 3 × 3√ 3), $\begin{pmatrix} 3 & 1 \\ 1 & 3 \end{pmatrix}$ and (2√ 3 × 2√ 3) patterns at θ_S > ¼ ML.[36-39] For S on Ru(0001), two phases were identified above θ_S= ⅓ ML - c(4 × 2) at θ_S= ½ ML and (√ 7 × √ 7) corresponding to θ_S= ⅜ ML.[40-44] On both Re(0001) and Ru(0001), all the reported high coverage phases is proposed to have pure S overlayer structure.

On the theory side, density functional theory (DFT) based investigations of S adsorption on metals such as Ag(111) [48], Ni(111) [49], Pt(111) [50,51] and Rh(111) [52,53] exist. This type of study is a valuable complement to experimental efforts since it allows direct determination of favorable binding sites and adsorption structures at the atomic scale. A preference for threefold hollow sites was found and a picture of strong binding of S on the metals has emerged, attributed to the overlap of S *p*-states with the metal surface *d* band. These

efforts, however, are focused largely on low coverages and complementary theoretical investigations of the experimentally observed high coverage phases are quite scarce.

The present work was undertaken to further improve the understanding of S adsorption on metal surfaces. In a previous paper, the experimentally detected low and high S coverage phases on Pd(111) were examined using first-principles DFT calculations.[54] This type of study has proved its worth in terms of complementing experimental efforts since it allows direct observation of the atomic positions. In the present paper, these investigations were extended to those observed on the Ag(111), Cu(111), Ni(111), Pt(111), Rh(111), Re(0001) and Ru(0001), focusing exclusively on the phases reported in experiments. Of particular interest is the determination of the energetics and geometries of structural models proposed in the experimental literature using a consistent theoretical scheme.

2. Computational approach

First-principles DFT total energy calculations were carried out using the Vienna *Ab Initio* Simulation Package (VASP) code.[55,56] The Perdew-Burke-Enzerhoff (PBE) generalized gradient approximation (GGA) [57] functional was employed to calculate the exchange-correlation energy. The electron-ion interaction was described by the projector-augmented wave (PAW) method.[58] The Kohn-Sham one electron valence eigenstates were expanded in terms of plane-wave basis sets with a cutoff energy of 280 eV.

The metal surface was modeled by a five-layer slab having a specified in-plane unit cell. Periodic boundary conditions were imposed in the two directions parallel to the surface (infinite in two dimensions). A 12 Å thick vacuum region is employed in order to ensure the decoupling of the consecutive slabs. For each surface, the lattice constant was fixed to the value obtained from optimizing with DFT this constant for the bulk metal. The computed lattice constants for the bulk fcc metals Ag, Cu, Ni, Pt and Rh are a = 4.17, 3.64,

3.52, 3.98 and 3.84 Å. They are found to within ~ 2% of the experimental values which are a_{exp} = 4.09, 3.61, 3.52, 3.92 and 3.80 Å.[59] For Re the calculated values of a = 2.77 and c =4.48 Å were applied, while for Ru, the values are a = 2.73 and c = 4.31 Å. These are in very good agreement with the values a_{exp}= 2.76 and c_{exp} = 4.46 Å (Re), and a_{exp} = 2.71 and c_{exp} = 4.28 Å (Ru) found in the literature.[59] On one side of the slab, pure S or mixed overlayer of S and metal atoms were added. The electrostatic potential is adjusted accordingly.[60] The construction of initial structure was guided by models proposed in the experimental literature. During the geometry optimization, atomic coordinates were allowed to relax except for the bottom two layers. The *k*-point sampling of the two-dimensional electronic Brillouin zone of the periodic supercells was performed using the Monkhorst-Pack scheme.[61] Monkhorst-Pack *k*-point mesh ranging from 1 × 5 × 1 to 7 × 7 × 1 was used depending on the dimension of the surface unit cell. A Methfessel-Paxton smearing [62] of σ = 0.2 eV was utilized to improve convergence and the corrected energy for σ → 0 was employed. Vibrational frequencies were calculated in order to ascertain the natures of the relaxed configurations. These calculations were performed by fixing the metal substrate in their relaxed positions and computing the normal mode frequencies of the overlayer atoms vibrating harmonically about their binding sites.

In the following, the manner in which the stability of the different model structures exhibiting particular translation symmetry would be compared is briefly discussed. The low coverage phases on Ag(111), Ni(111), Pt(111), Rh(111), Re(0001) and Ru(0001), and the high coverage ones on Ag(111), Pt(111), Rh(111), Re(0001) and Ru(0001) have pure S overlayer structures. In such cases, the commonly used binding energy per number of S atom, E_{bind} , was calculated. It is defined as

$$E_{bind} = (E^{slab}_{S/surface}(N_S) - E^{slab}_{surface} - N_S E_S)/N_S\,, \qquad (1)$$

where $E^{slab}_{S/surface}$ and $E^{slab}_{surface}$ are the total energy of the adsorbed system and bare surface, respectively. The term N_S is the number of S atoms while E_S is the total energy of a S atom. However, for cases where mixed S-metal overlayer structure is present such as the high coverage phases on Cu(111) and Ni(111), Eq. 1 cannot be used. Following previous work [54], the energetics was determined on the basis of the binding energy per surface unit cell (referred here as E_{bind}') :

$$E_{bind}' = (E^{slab}_{S-M/surface}(N_S, N_M) - E^{slab}_{surface} - N_M E^{bulk}_M - N_S E_S). \quad (2)$$

Here $E^{slab}_{S-M/surface}$ is the total energy of the adsorbed system and bare surface, N_M is the number of metal overlayer atoms in addition to the bare surface and E^{bulk}_M is the total energy of a *M* metal atom in bulk metal *M*. It should be noted that E_{bind}' as defined above is related to E_{bind} in Eq.1 by multiplying the former by $1/N_S$ and setting N_M to zero.

3. Results and discussion

3.1 Low coverage phases – pure S overlayer

The lowest energy structures of the low coverage phases with simple S overlayer structures reported from experiments were determined. They are the (2 × 2) phase with θ_S = ¼ ML for S on Ni(111), Pt(111), Re(0001) and Ru(0001) and the ($\sqrt{3} \times \sqrt{3}$) phase in Ag(111), Ni(111), Pt(111), Rh(111) and Ru(0001) at θ_S = ⅓ ML. Additionally, the c($\sqrt{3} \times 5$) phase on Re(0001) detected at θ_S= ⅕ ML was also examined. Structures with the adsorbate occupying high symmetry sites on the surface unit cell were explored. Given one S atom in the unit cell, four high symmetry sites are possible: top, bridge, hcp and fcc (see Supporting information). The predicted binding energies and optimized structural

parameters are tabulated in Table 1. The binding energies were also plotted in Fig.1 for clarity.

For the Re(0001)-c(√ 3 × 5)S, only the fcc and hcp sites were found to be stable adsorption sites. This is not the case for top and bridge site adsorption since the atom on these sites moved to an adjacent hollow site in the course of structural optimization. The hcp site shows the stronger binding energy with the fcc site 0.27 eV less stable. For all the (2 × 2) phases, adsorption on the threefold hollow sites is predicted to be the more favorable with the preference changing from the hcp site on the (0001) surface to the fcc site on the (111) surface. The fcc site on Ni(111) and Pt(111) is more preferred over the hcp site by 0.05 – 0.20 eV while on Re(0001) and Ru(0001), hcp is favored by 0.12 – 0.25 eV. This binding trend is generally seen as well on the various (√ 3 × √ 3) phases examined here. It should be noted that for both (2 × 2) and (√ 3 × √ 3) phases, the bridge site is predicted to be a transition state on the basis of vibrational frequency calculations. By contrast, the top site is a higher order rank-2 saddle point. Altogether, the site determination is consistent with the typical pattern of preferred occupancy of threefold hollow sites at low coverages, notably the fcc site on the (111) surface and the hcp site on the (0001) surface – sites that the next layer would occupy.[18,19,21,23,25,28-31,36-40,63,64]

In an earlier work, DFT investigations of S on Ag(111) with hypothetical (3 × 3) periodicity (θ_S = ⅑ ML) were reported.[65] The fcc site was identified as the most stable with calculated binding energy of E_{bind} = -3.94 eV. This is more exothermic compared to the value of -3.69 eV for Ag(111)-(√ 3 × √ 3)S which is attributed to the fact that the (√ 3 × √ 3) phase has a higher coverage. Experimental studies for this system for which to compare the calculated geometrical parameters are not available. Previous DFT studies of the Ni(111)- (2 × 2)S also identified the fcc hollow site as the most preferred.[66] The reported

LEED S-Ni bondlengths range from 2.02 ± 0.06 Å to 2.23 ± 0.02 Å [18,19,25,63]. Ion scattering studies yield a value of 2.16 ± 0.04 Å [21] and NIXSW studies reported a value of 2.11 ± 0.03 Å.[23] The calculated value of 2.14 Å is within the experimental range. For the corresponding Ni(111)-($\sqrt{3} \times \sqrt{3}$)S, the EXAFS determined S-Ni distance of 2.13 Å [67] agrees well with the predicted value.

DFT investigations of Pt(111)-(2 × 2)S was previously undertaken and these calculations also identified the fcc site as the most stable for S adsorption. The corresponding binding energies are E_{bind} = -4.55 [68] and -5.14 eV eV [51]. The computed value of -5.23 eV found here is larger which could be due to some differences between the calculational details underlying these studies. The S-Pt bond length of 2.28 Å found for both Pt(111)-(2 × 2)S and Pt(111)-($\sqrt{3} \times \sqrt{3}$)S is slightly longer by 0.03-0.04 Å compared to the LEED values found by Yoon *et al*. [31] For Rh(111)-($\sqrt{3} \times \sqrt{3}$)S, the LEED S-Rh bondlength considering fcc site adsorption is reported.[31,35] The values are 2.23 and 2.25 ± 0.04 Å which compares well with the prediction of 2.27 Å.

For Re(0001)-c($\sqrt{3} \times 5$)S, the S atoms are largely grouped into rows and the distance between S is about $\sqrt{3}$ times the Re-Re bondlength. A preference for hollow site was suggested in previous experiments but there was no conclusive evidence as to which of the two inequivalent hollow sites the S is situated at.[36] In this work, it was predicted that that hcp site is more favored than fcc by 0.27 eV. For the corresponding Re(0001)-(2 × 2), hcp is also the most favored site from the energetic standpoint. The vertical distance of the S atoms from top layer substrate center of mass is 1.72 Å which compares well with the reported LEED value of 1.67 Å.[38] On Ru(0001), LEED studies considering hcp site adsorption yielded S-Ru bond length of 2.29 ± 0.02 Å and 2.28 ± 0.02 Å for the (2 × 2) and ($\sqrt{3} \times \sqrt{3}$) phases, respectively.[40] The calculated value here of 2.33 Å for both phases is slightly longer by 0.04-0.05 Å.

For the various ($\sqrt{3} \times \sqrt{3}$) phases examined, no adsorbate induced buckling is detected in the first layer of the substrate because it is symmetry forbidden. However, for the c($\sqrt{3} \times 5$) and (2×2), buckling is predicted to occur with values Δz_1= 0.05-0.15 Å. Examination of the relaxed structures indicate that it is due to the lifting up of the three metal atoms bonded to S accompanied by downward movement of the remaining under-coordinated atoms. This behavior is consistent with available LEED data tabulated in Table 1. For Pt(111)-(2×2)S and Ru(0001)- (2×2)S, the reported values are $\Delta z_1 = 0.08 \pm 0.04$ Å [31] and $0.030^{+0.015}_{-0.030}$ Å [40], while the calculations yielded 0.15 Å and 0.09 Å, respectively. For the (111) surfaces, small expansion of the first interlayer spacing for up to $\Delta_{12} = 1.8$ % with respect to the bulk value was found. The opposite behavior is seen in the hcp metals which yield Δ_{12}= -2.1 – -5.1 %. For Ni(111)-(2×2)S, Ni(111)-($\sqrt{3} \times \sqrt{3}$)S and Rh(111)-($\sqrt{3} \times \sqrt{3}$)S, the contraction of the outermost interlayer spacing that occurs in the clean surface was completely removed in the adsorbed system. For the hcp metals, this contraction was not removed by S adsorption. The calculated values of Δ_{12} support the available LEED finding of small expansion of the interlayer spacing found in Ni(111)-(2×2)S, Pt(111)-(2×2)S and Pt(111)-($\sqrt{3} \times \sqrt{3}$)S, and the opposite effect in Re(0001)-(2×2)S, Ru(0001)-(2×2)S and Ru(0001)-($\sqrt{3} \times \sqrt{3}$)S (see Table 1).

3.2 High coverage phases -pure S overlayer

3.2.1 Sulfur on Ag(111)

The equilibrium geometry of the Ag(111)-($\sqrt{7} \times \sqrt{7}$)-S structure derived from the model suggested by Schwaha *et al.* [8], Rovida and Pratesi [9], and by Heinz and Rabe [10] was determined. Following their proposal, one of the S atom per unit cell was initially placed above the top site and the others are on the hcp and fcc sites ($\theta_S = 3/7$ ML). The optimized

geometry is shown in Fig. 2a ($S_{top}S_{fcc}S_{hcp}$). The S atoms remain at the top, fcc and hcp sites. It should be noted, however, that $S_{top}S_{fcc}S_{hcp}$ is not a minimum. It was predicted as a higher order (rank-2) saddle point.

The second model favored by Aloisi *et al* [11] ($\theta_S = 3/7$ ML) differs in terms of the arrangement of the three S atoms per unit mesh. Additional data from a high resolution analysis of the bright spots in the STM image indicates the existence of adsorbed S_3 cluster within the unit cell. Like the ground state structure of S_3 known to assume a triangular shape in the vapor phase [69], the trimers retained the same shape with two sides of equal length. However the reported lengths are not consistent with the picture of interacting S_3 cluster since they are significantly different from their vapor phase counterpart. They reported two sides of length 2.60 Å and one of length 3.82 Å, significantly larger than the values 1.93 and 3.31 Å found for the vapor phase molecule.[69] It was also conjectured that the trimer is centered around the top site of the substrate lattice. To verify this, two structures were optimized consisting initially of S on the three nearest neighbor fcc and hcp sites with the S atoms arranged around a top site. It should be noted that other possible initial geometries involving three S atoms around a top site exist, but it was found unnecessary to consider them in light of what was learned from these examined representative structures. It was found that interacting S_3 cluster situated around a top site is not stable. The S atoms moved away from each other and relaxed towards neighboring bridge sites after relaxation of the atomic positions as shown in Figs. 2b-c (S_{3fcc} and S_{3hcp}). While these structures are predicted to be local minima, the trimer is non-interacting judging from the large S-S distances of 4.36-4.40 Å. Thus, further DFT examination of this trimer based model is called for.

It was found previously that the preferred structure for S_2 on close-packed (111) metal surface consists of one S atom on a top site and the other one on the second nearest neighbor bridge site.[70-72] Using this as a starting point, another S on the unit cell was placed to search for a potential structure for a triangular, interacting S trimer. An energetic minimum was found and the most preferred structure consists of an S atom on the top site bonded to two S atoms situated on off-bridge site positions (Fig.2d, $S_{top}S_{2brg}$). In line with the STM results, the trimer is triangular in pattern. It lies nearly parallel to the surface with two sides of equal length. Moreover, the trimer is interacting based on calculated bond lengths. The calculated S-S bond distance of 2.09 Å is fairly close to the vapor phase S_3 which is 1.93 Å. The calculated length for the long side is 3.47 Å, 0.16 Å larger compared to the free molecule. Based on calculated E_{bind} (see Table 2), this structure is more energetically favorable than model S_{3fcc}, S_{3hcp} and $S_{top}S_{fcc}S_{hcp}$.

3.2.2 Sulfur on Pt(111), Rh(111), Ru(0001) and Re(0001)

On Pt(111), LEED data indicate adsorbed S with $(7 \times \sqrt{3})$ periodicity at $\theta_S = 3/7$ ML.[28,31] On Rh(111), both $(7 \times \sqrt{3})$ ($\theta_S = 3/7$ ML) and c(4 × 2) ($\theta_S = 1/2$ ML) phases were detected.[32-35] In the case of Re(0001), the reported three phases at $\theta_S > 1/4$ ML are $(3\sqrt{3} \times 3\sqrt{3})$, $\begin{pmatrix} 3 & 1 \\ 1 & 3 \end{pmatrix}$ and $(2\sqrt{3} \times 2\sqrt{3})$ in order of increasing coverage, [36-39] while LEED data indicate a c(4 × 2) at $\theta_S = 1/2$ ML and $(\sqrt{7} \times \sqrt{7})$ at $\theta_S = 4/7$ ML for Ru(0001).[42-44] All of these phases were reported experimentally to possess pure simple S overlayer structures. To the author's knowledge, the various models proposed in the literature have not been examined theoretically. Based on the available structural information from experiments, S adsorption on the above metals was investigated using appropriate surface unit cells. The calculated energetics and geometrical parameters are tabulated in Table 2.

For Pt(111)-(7 × √ 3)S, it was suggested that one of the S atoms in the unit cell is on the hcp site while the other two are situated on the next nearest fcc sites.[28,31] Starting from this configuration, an energetic minimum for this three S atom model after geometrical optimization was found (Fig. 3a). This work provides theoretical confirmation for the experimentally observed height difference between the S at the fcc and hcp sites. S on hcp is 0.11 Å higher than on the fcc which is close to the value of 0.15 Å estimated from STM data [31]. An alternative (7 × √ 3) phase was explored with the arrangement of S analogous to Fig. 3a but with 1:2 occupation of the fcc and hcp site position. The resulting structure (Fig. 3b), however, is less favorable by 0.05 eV based on DFT. Moreover, the S atoms are nearly coplanar since no noticeable variation in their heights was found.

The S occupancy in Rh(111)-(7 × √ 3)S was conjectured to be similar to its Pt(111)-(7 × √ 3) counterpart, while for the c(4 × 2) phase, 1:1 occupation of the fcc and hcp sites was proposed. The relaxed (7 × √ 3) phase starting from S on the fcc and hcp sites with 2:1 occupation is given in Fig.4a. The same phase with 1:2 S occupation of fcc and hcp sites was also explored (Fig. 4b). The two model structures differ by only 0.01 eV so they are likely to co-exist at $\theta_S = 3/7$ ML. Low temperature LEED analyses may be able to distinguish between the two structures. Unlike Pt(111)-(7 × √ 3)S, detailed structural information for this phase from experiments are not reported and as a result, any quantitative comparison cannot be made. For the c(4 × 2) phase, initial structure was optimized with S at the ideal fcc and hcp sites and it was confirmed that such mixed configuration is indeed a local minimum (Fig.4c, $S_{fcc}S_{hcp}$). Alternate model with S on hcp and top sites ($S_{hcp}S_{top}$), and S on fcc and top ($S_{fcc}S_{top}$) sites were tested. They are found to be unfavorable by 0.82-0.83 eV compared to model $S_{fcc}S_{hcp}$ (Fig 4c). Moreover,

vibrational frequency calculations indicated that these structures are not minima but rank-2 saddle points.

Foord *et al.* observed a (4 × 4) phase on Rh(111) using LEED with further S_2 dosing and annealing of the c(4 × 2) overlayer to 600 K.[33] Yoon *et al.* also detected this phase with LEED when the c(4 × 2) phase was heated above 900 K.[34] The suggested model is a simple S overlayer structure with coverage similar to the c(4 × 2). The eight S atoms in the unit cell occupy only one type of hollow site - seven of them arranged in a diamond-like configuration plus a common corner S lying at the lattice points. Starting from this configuration with S on the fcc sites, DFT calculations were carried out and the energetic minimum is displayed in Fig. 4d. This model was predicted to be less stable by 0.18 eV compared to the c(4 × 2) overlayer. A counterpart structure with S on the hcp site is also found to be equally unfavorable. The reduction in stability reflects the relatively more enhanced repulsive lateral interaction within this denser overlayer. Examination of the Fig. 4d, for example, reveals that though the overall diamond like configuration of the interior S atoms (S_2-S_8) was retained, some of them do not prefer to stay on the fcc sites. Six of the S atoms per unit cell ($S_{2\text{-}4}$ and $S_{6\text{-}8}$) are significantly more displaced from the center of the fcc sites in order to reduce steric repulsion. It should be noted that Yoon *et al* discuss the possibility that the (4 × 4) phase may not be a simple S overlayer structure but involves reconstruction of the underlying metal substrate in order to offset the enhanced S-S repulsion.[34] Foord *et al*. went on further by favoring a model that consists of mixed overlayer structure.[33] However, no detailed structures were provided for such alternate scenario and further analysis of the (4 × 4) phase cannot be carried out in the absence of more concrete information.

For Re(0001)-(3√ 3 × 3√ 3)S with θ_S = 4/9 ML, groups of three S atoms in hcp sites were placed on the surface unit cell, forming an arrangement of triangles. Three groups are centered around a fcc site (fcc site trimer) while the other one is centered around a top site (top site trimer). The reported coverage for the $\begin{pmatrix} 3 & 1 \\ 1 & 3 \end{pmatrix}$ phase is θ_S = ½ ML and the initial structure consists of diamond shaped aggregate of four S atoms (tetramer) on the hcp sites. The (2√ 3 × 2√ 3) phase has a reported coverage of θ_S = ½ ML as well. Six S atoms (hexamer) on the hcp site were placed on the unit cell forming an arrangement of hexagons. All these starting geometries are consistent with models proposed from experiments.[36-39] For comparison, the corresponding structural counterparts of each phase where S atoms reside on the fcc sites were also examined. The DFT relaxed structures are shown in Figs. 5a-5c. The results provide theoretical confirmation that hcp site adsorption is the more preferable for these phases. They are predicted to be favorable by 0.25 – 0.30 eV compared to fcc site adsorption (see Table 2). The two phases, $\begin{pmatrix} 3 & 1 \\ 1 & 3 \end{pmatrix}$ and (2√ 3 × 2√ 3), with similar coverage of θ_S = ½ ML are close in energy. The calculated energy difference between them is only 0.02 eV and this could be the reason why they are observed to co-exist at θ_S = ½ ML. The computed S-S distances indicate that the trimer, tertramer and hexamer structures observed on Re(0001) are non-interacting. Vapor phase S_n (n=3-20) with ring-like structures have bondlengths in the 1.93-2.05 Å range.[69,73] However, the predicted values in the (3√ 3 × 3√ 3), $\begin{pmatrix} 3 & 1 \\ 1 & 3 \end{pmatrix}$ and (2√ 3 × 2√ 3) phases are significantly larger: 3.19-3.30 Å, 3.15-3.23 Å and 3.05-3.06 Å, respectively.

For Ru(0001)-c(4 × 2)S, it was proposed that the unit cell contains two S atoms and the proposed model consists of equal occupation of the fcc and hcp sites ($S_{hcp}S_{fcc}$) as in the c(4 × 2) phase on Rh(111).[42] Model with S on hcp and top sites ($S_{hcp}S_{top}$) and another one with fcc and top sites ($S_{fcc}S_{top}$) occupied were tested as well but they were ruled out on the basis

of quantitative LEED analysis. The DFT calculations found an energetic minimum for the $S_{hcp}S_{fcc}$ model (Fig.6a). The $S_{hcp}S_{top}$ and the $S_{fcc}S_{top}$ models were predicted to be transition states. For the ($\sqrt{7} \times \sqrt{7}$) phase, STM, LEED and Auger data revealed that the unit cell contains four atoms.[42,74] Following the model of Sklarek *et al* .[43], structure with S occupation of three hcp and one fcc sites ($S_{3hcp}S_{fcc}$) was optimized where three of S atoms that occupy the hcp sites are in a triangular-like arrangement. A second model with the occupation numbers interchanged ($S_{3fcc}S_{hcp}$) was also considered for comparison. Energetic minimum was found for these structures. The $S_{3hcp}S_{fcc}$ model (Fig. 6b) based on the proposal by Sklarek *et al.* is predicted to be slightly stable by 0.03 eV.

For the pure S overlayer structures examined here, a decrease in the binding energy with increasing S coverage is observed (Fig. 7). This weakening of the adsorbate-metal bond reflects the enhancement of repulsive lateral interaction as the S overlayer becomes more densely packed. The relaxation pattern for the higher coverage phases is slightly more complex than their low coverage counterparts. On Pt(111), Rh(111), Re(0001) and Ru(0001), the S atoms are laterally shifted off from their respective ideal hollow site position in view of the enhanced repulsive lateral interactions at higher coverages. The S displacement on these surfaces are in the 0.25 − 0.33, 0.18 − 0.57, 0.24 − 0.32 and 0.17 − 0.34 Å range. For Ru(0001)-c(4 × 2)S, the TLEED determined S lateral displacement of 0.10 − 0.18 Å [44] is in agreement with the value of 0.15 − 0.18 Å. For Re(0001)- ($2\sqrt{3} \times 2\sqrt{3}$)S, the predicted value of 0.25 Å is larger than the reported value of ~ 0.4 Å.[38] One source of deviation could be attributed to the fact that in the TLEED fitting process, the S atoms were assumed to be distorted with long and short distances of 3.32 and 2.95 Å, respectively. The calculations do not offer support that the S hexamer in Fig 6c is distorted since the predicted S-S distances are essentially of uniform length (3.05-3.06 Å).

S induced buckling of the outermost layer of the substrate is predicted due to difference in the height the metal atoms. The larger the S coordination, the more pronounced the vertical displacement of the atoms away from the bulk. For example, in Re(0001)- ($3\sqrt{3} \times 3\sqrt{3}$)S (Fig. 5a), Re(0001)-$\begin{pmatrix} 3 & 1 \\ 1 & 3 \end{pmatrix}$S (Fig. 5b), and Ru(0001)-($\sqrt{7} \times \sqrt{7}$)S (Fig. 6b), the two-fold S and three-fold S coordinated metal are positioned 0.17 and 0.28 Å, 0.16 and 0.31 Å, and 0.20 and 0.63 Å, above the one-fold S-coordinated atom. The results are in reasonable agreement with available experimental data. For Ru(0001)-c(4 × 2)S, the TLEED determined buckling is 0.19 ± 0.02 Å [44] while the predicted value is 0.21 Å. For Ru(0001)-($\sqrt{7} \times \sqrt{7}$)S, the reported buckling between three-fold and two-fold S coordinated metal atoms and between two-fold and one-fold S coordinated metal atoms are 0.39 ± 0.02 and 0.18 ± 0.02 Å [44] which compare well the predicted values of 0.42 and 0.20 Å.

Although surface buckling and lateral shifts of S atoms occur, the local threefold coordination of the S atoms is essentially retained. However, the bond length slightly varies depending on the nature of metal atoms involved in the bonding. Overall, it was found that S-metal bond length increases slightly with increasing S-coordination of the metal. This trend is consistent with available published experimental data.[44] In the LEED studies of Ru(0001)-c(4 × 2)S, it was reported that the S atom close to the hcp site has a bond of 2.26 and 2.29 Å with the onefold and twofold S coordinated metal while the S atom close to the fcc site has a bond of 2.24 and 2.28 Å, respectively. The predicted values for S close to the hcp site are 2.27 and 2.33 Å, while they are 2.30 and 2.32 Å for the other S. For the corresponding ($\sqrt{7} \times \sqrt{7}$) phase, the reported bondlengths between S and its nearest neighbor metal atoms are 2.23 ± 0.05 (onefold S bonded Ru), 2.26 – 2.27 ± 0.05 (twofold S bonded Ru) and 2.33 ± 0.05 Å (threefold S bonded Ru) while the values are 2.26, 2.28-2.32 and 2.35 Å, respectively. TLEED data for Re(0001)-($2\sqrt{3} \times 2\sqrt{3}$)S is also reported and it

was determined that each S atom makes two short bonds (2.21 and 2.24 Å) and one long bond (2.51 Å) with the surface.[38] In this work, each S atom in Fig. 5c was also found to form short and long bonds with the substrate, but the results differ in terms of the number of them. One short bond (2.34 Å) between the S and the onefold S coordinated metal was found and two longer ones (2.39 and 2.45 Å) which involved bonds with the twofold S coordinated metal atoms. The discrepancy may be due to the structural constraint imposed in the arrangement of S hexamer in the previous work when the TLEED analysis was done.[38]

3.3 High coverage phases - mixed S-metal overlayer

3.3.1 Sulfur on Cu(111)

Various models for the ($\sqrt{7} \times \sqrt{7}$) structure of S on Cu(111) proposed in the literature were investigated. One model supported by Domangue and Oudar and Prince *et al.* consists of three S and three Cu atoms per unit cell ($\theta_S = 3/7$ ML).[12,13] Following their work, two S atoms were initially placed on the fcc and hcp sites and the other on the top site. The three Cu atoms were added into the hollow-like position created by the S atoms (i.e. bridge sites with respect to the top Cu substrate layer) forming a hexagonal S-Cu overlayer. An energetic minimum was found for this model and the DFT optimized geometry is shown in Fig. 8a (*Prince* model). It was found that the two of the S atoms remain on the fcc and hcp sites while the other one remains on the top site. Furthermore, the three Cu atoms are situated on slightly off-bridge site positions. The SEXAFS and NIXSW studies by Prince *et al.*.[13] reported only one value for nearest neighbor S-Cu distance (2.30 Å). It was suggested, however, that there could possibly be two or more slightly different values and this work offer theoretical support to this particular scenario in view of the fact that the S

atoms occupy different high symmetry sites. The S on the top, hcp, and fcc sites were found to have three nearest Cu neighbors in the overlayer region at lateral distance of $d(S_{top}\text{-Cu})$ = 2.22 Å, $d(S_{hcp}\text{-Cu})$ =2 .37 Å, $d(S_{fcc}\text{-Cu})$ = 2.27 Å, respectively. The S overlayer is predicted to be distorted and the calculated buckling between S atoms and the top Cu substrate are $\Delta z_1(S_{top}\text{-Cu})$ = 2.52 Å, $\Delta z_1(S_{hcp}\text{-Cu})$ =2 .05 Å and $\Delta z_1(S_{fcc}\text{-Cu})$ = 1.91 Å. To determine the vertical distance, the center of mass of the metal layer is used. The reported experimental values are 2.30, 1.77 and 1.77 Å, respectively. The deviations between the calculations and the experiments could be attributed to the fact that the Cu substrate atoms were not allowed to relax in the fitting of the SEXAFS data.[13] Moreover, the S atoms on both hollow sites were constrained to be coplanar during the fitting process. These types of structural constraints were not imposed in the calculations.

The model proposed by Foss *et al.* based on an S atom adsorbed on a square-like Cu_4 fragment above the top layer metal substrate was considered next.[15,17] Additionally, two lower S atoms are on the hcp and fcc sites per unit mesh giving rise to $\theta_S = 3/7$ ML. It should be noted that the locations of the four metal atoms in Cu_4S group were not clearly resolved in their model. Here, an initial geometry involving four Cu atoms around a top site was constructed. In particular, an arrangement consisting of a pair of Cu atoms on two opposite nearest neighbor top sites and the other pair on the two second nearest neighbor bridge sites yields a roughly square shaped Cu_4 cluster on the surface. An S atom was added on the fourfold hollow created by the cluster forming a Cu_4S fragment on the surface. Two additional S atoms were placed on the hcp and the fcc sites to complete the starting structure. An energetic minimum was found with the Cu_4S group remaining intact after full relaxation of the atomic positions (Fig. 8b, *Foss* model). The Cu_1-Cu_4 atoms are either at off-top or off-bridge site position, forming an approximately coplanar square cluster. S_{top} is

four-fold coordinated to this structure while the lower S_{hcp} and S_{fcc} atoms remain on the hcp and fcc sites.

The model suggested by Saidy and Mitchell which consists of three Cu overlayer and three S atoms in the unit cell was considred.[16] Following their work, an initial structure with three Cu atoms on the fcc sites forming an arrangement of triangles was constructed. The substrate metal atom immediately below the threefold hollow site created by these upper Cu atoms was replaced by a S atom (forming a local Cu_3S fragment) with the two remaining S atoms were placed on the hcp and fcc sites. This initial model which amounts to S atoms replacing substrate metal atoms was predicted to be extremely unstable, inducing very large structural distortions. In particular, the relaxed structure is characterized by significant vertical and lateral displacements of the embedded S atom and the overlayer Cu atoms, respectively (Fig. 8c, *Saidy* model). The optimized structure roughly resembles the *Prince* model but with one substrate Cu atom missing per unit mesh. The binding energy per surface unit cell, E_{bind}', for all the examined ($\sqrt{7} \times \sqrt{7}$) structures are given in Table 3. It can be seen that DFT calculations predict the *Prince* model to be the most energetically favorable, with the other models disfavored by 0.11−1.31 eV.

3.3.2 Sulfur on Ni(111)

For Ni(111)-($5\sqrt{3} \times 2$)S, a trial geometry that consist of a16 atom Ni overlayer with an essentially (100)-like geometry on a ($5\sqrt{3} \times 2$) unit cell was set up.[24-27,47] The Ni-Ni distance along the $5\sqrt{3}$ direction was stretched by about 0.3 Å with respect to the bulk value to match the length of the long axis of the rectangular unit mesh. The eight S atoms were placed on alternate fourfold coordinated hollow adsorption sites created by the metal overlayer to form a structure that has a c(2 × 2) periodicity with respect to this overlayer. From this, additional initial structures that maintain the relative positions of the atoms in

the overlayer, but testing different lateral positions for the overlayer with respect to the underlying substrate, were generated. That is, structural optimization of various starting geometries arising from incremental lateral shift of the overlayer by up to $0.4\,\vec{a}$ and $0.1\,\vec{b}$, where $\vec{a}$ and $\vec{b}$ are the lattice vectors of the short and long direction of the rectangular surface mesh, respectively, was carried out.

The calculations yielded two stable low energy structures shown in Figs. 9a-b and their energies are listed in Table 4. In both cases, the Ni overlayer did not remain in a nearly square unit mesh configuration as in Ni(100). On the other hand, the overlayer is severely reconstructed from this pseudo-(100) model. The structure in Fig. 9a, in particular, referred to as model C_1 is compatible with the clock reconstructed model previously proposed.[23,46] It involves concerted rotation of two pairs of square like tetramers, Ni_1-Ni_4, Ni_5-Ni_8, Ni_9-Ni_{12} and Ni_{13}-Ni_{16} in alternate clockwise and counterclockwise direction. The rotation was predicted to be $\sim \pm 16°$ with respect to $\vec{a}$ compared to $\sim \pm 14°$ estimated from experiments.[46] Three atoms per tetramer (Ni_1-Ni_3, Ni_5-Ni_7, Ni_9-Ni_{11} and Ni_{14}-Ni_{16}) are situated on off-hollow site positions and threefold coordinated with the underlying Ni(111) substrate. The other Ni (Ni_4, Ni_8, Ni_{12} and Ni_{13}) are on an off-bridge site and only two-fold bonded with the substrate. To compensate for this, formation of additional Ni_4 −Ni_8 and Ni_{12}−Ni_{13} bonds occurs.

Two S adatoms per unit mesh (S_1 and S_3) were predicted to drop into deeper lying sites on the surface in regular rows along $\vec{b}$. This picture is consistent with the experimental observation that every fourth S adatom along the long direction of the surface unit cell penetrate the pseudo(100) layer to bond to the underlying substrate.[23] The fourfold coordinated S_2, S_4, S_5, S_6, S_7 and S_8 atoms are 3.25 Å above the Ni(111) substrate while the S_1 and S_3 atoms are located 0.76 Å lower. The corresponding measured values are 3.28 ±

0.1 Å and 0.8 ± 0.1 Å, respectively. This work provides theoretical support for the suggestion of Lüdeke *et al.* [23] that the clock-like modification of the Ni overlayer accounts for lowering of this subset of S atoms. In particular, it was found that one side of the fourfold coordinated hollows on which these lower S atoms are situated to be relatively "enlarged". This caused the S_1 and S_3 atoms to drop towards the substrate, creating a fifth bond with metals on the metal substrate, in addition to the four bonds with the metal overlayer. In the case of the Ni(111) substrate, no severe structural distortion was observed. The only noticeable perturbation is that this layer is corrugated due to the fact that the substrate atoms which interact with S_1 and S_3 are displaced upwards by ~ 0.3 Å with respect to the other ones.

The other structure is displayed in Fig. 9b (model *C_2*). It is slightly less favorable by 0.03 eV. Similar to model C_1, ¾ of the overlayer Ni are threefold coordinated while the remaining ¼ are twofold coordinated to the substrate. Moreover, two S adatoms per unit mesh also dropped to a lower S-substrate layer spacing relative the other S. The major difference between the two structures is the arrangement of the overlayer. The tetramer pair, Ni_1-Ni_4 and Ni_5-Ni_8 are rotated clockwise while Ni_9-Ni_{12} are in the counterclockwise direction as in model *C_1*. The other tetramer Ni_{13}-Ni_{16}, however, is now enlarged with the S atom above it (S_8) dropping towards the substrate and creating a fifth bond with a metal on the Ni(111) substrate. The other dropped S (S_3) is situated on the upper portion of the unit cell. A clear implication of the present result is that model *C_2* may coexist with model *C_1* since their energy difference is not very significant, and it may be unlikely that only one structural type of $(5\sqrt{3} \times 2)$-S phase on Ni(111) would be present. Low temperature LEED analyses may be able to distinguish between there two structures.

3.4. Electronic properties

The presence of the overlayer results in noticeable changes in the metal substrates electronic structure. This is illustrated in Figs.10-11 by the partial electronic density of states (PDOS) of selected low and high coverage pure S overlayer on Pt(111) surface (Pt(111)-(2 × 2)S and Pt(111)-(7 × √ 3)S). In Fig. 12, the corresponding calculated PDOS for a system which involved the presence of mixed S-metal overlayer (Cu(111)-(√ 7 × √ 7)S, *Prince* model) is also displayed. For reference, the PDOS of the bare surfaces are also shown in these figures. The electron energies are given with respect to the Fermi level. Results for these representative cases were only shown for the sake of keeping the paper within a limited length. In Figs.10-11, the presence of adsorbed S overlayer broadens the surface Pt *d* band and reduces the value of DOS at the Fermi level. This is due to the increase in the coordination of surface Pt atoms in the adsorbed system. For Pt(111)-(2 × 2)S (Fig. 10), the interaction of the adsorbate with the surface gives rise to diffused features in the region from -5.2 to -7.3 eV which consist of overlapping Pt *d* split-off states and S *p*, plus some contribution from Pt *s*. The broad S *p* peak at around ~ 5.9 eV found in Pt(111)-(2 × 2)S becomes more broadened for the higher S coverage Pt(111)-(7 × √ 3)S structure. Additionally, a noticeable splitting is seen in the lowest lying S *s*. This is in contrast to the Pt(111)-(2 × 2)S case where a relatively more defined peak due to S *s* is observed. This is in line with the enhanced interaction between the S adatoms for this more densely packed overlayer.

A number of similar observations can be made for the PDOS of the most energetically favorable model for the (√ 7 × √ 7) phase on Cu according to Prince *et al*. (Fig. 12). For example, the *d* band for the adsorbed system is also noticeably broadened relative to the bare surface, indicating rehybridization of the surface *d* band and the delocalized bonding S *p* states. Interaction between the extended occupied band of the Cu overlayer which has

primarily *d* character (but with weaker split-off states) with the metal subsrate is also detected. The interactions with the mixed Cu-S overlayer induce an increase of the DOS for the energetically lower part of the substrate *d* band. It is also interesting to note that below the Fermi level, the S *p* and Cu *d* in the overlayer region have overlapping features. This, plus the fact that a noticeable splitting is seen in the lowest lying S s states, are indicative of interaction between the S and Cu atoms in the overlayer.

Estimation of nature of S-metal surface interactions is carried out using Bader charge analysis.[75,76] The calculated total valence electronic populations N_e of adsorbed S in various ground state low ($\leq \frac{1}{3}$ ML) and high coverage ($> \frac{1}{3}$ ML) phases on metals are presented in Fig. 13. If the values of the charge on the adsorbed S for the low coverage pure overlayer phases are calculated (N_e minus the number of S valence electrons corresponding to 6), it is evident that the interaction of S with Pt and Rh results in a generally covalent bonding. The charge on S ranges from ~ 0 to 0.22|*e*|. For Ag, Ni, Re and Ru, on the other hand, the interaction has a larger ionic character with a net charge on S in the range 0.38|*e*| to 0.56|*e*|. The most ionic interaction is that with the Ag and Re metals and the least ionic is that with the Pt metal. The nature of S-metal interaction for Rh, Ni and Ru is intermediate between the two limiting situations represented by Ag, Re and Pt.

When comparing the charge values between the low and high coverage *pure* overlayer phases on Ag, Re and Ru, it was found that the bonding in the high coverage exhibits relatively less ionic character. That is, for a given metal, a noticeable decrease in the Bader net charge of the high coverage phases was observed compared to their low coverage counterparts. On Ag, Re and Ru, the average charge on S at low coverage are 0.51|*e*|, 0.55|*e*|, and 0.39|*e*|, whereas the average values for the corresponding high coverage phases are 0.20|*e*|, 0.48|*e*|, and 0.29|*e*|, respectively. The reduction in ionicity at higher coverage

serves to minimize the Coulomb repulsion in the overlayer. This trend, however, is not observed for S on Pt and Rh which exhibit generally covalent bonding at all coverages.

For Cu(111)-($\sqrt{7} \times \sqrt{7}$)S (*Prince* model) and Ni(111)-(5$\sqrt{3} \times 2$)S (C_1), both mixed overlayer structures show that the most significant charge variation occurs in the overlayer region. The S atoms gain charge and again behave as electronegative adsorbates. On the other hand, the observed charge transfer for the adjacent metal atoms is in the opposite direction, with Cu and Ni overlayer atoms losing 0.58|*e*| and 0.18|*e*| - 0.23|*e*|, respectively. The interactions exhibiting the largest degree of ionicity is found for S in Cu(111)-($\sqrt{7} \times \sqrt{7}$)S with S charge values of 0.64|*e*| - 0.70|*e*|. The corresponding bonding in Ni(111)-(5$\sqrt{3} \times 2$)S has less ionic character with a S charge values of 0.39|*e*| - 0.50|*e*|.

4. Conclusion

In summary, the results of first-principles density functional theory investigations addressing the structure of S on Ag(111), Cu(111), Ni(111), Pt(111), Rh(111), Re(0001) and Ru(0001) surfaces were reported. The adsorption geometry of the sulfur atom in the experimentally observed c($\sqrt{3} \times 5$) phase ($\theta_S = \frac{1}{5}$ ML) on Re(0001), (2 × 2) phase ($\theta_S = \frac{1}{4}$ ML) on Ni(111), Pt(111), Re(0001) and Ru(0001), ($\sqrt{3} \times \sqrt{3}$) phase ($\theta_S = \frac{1}{3}$ ML) on Ag(111), Ni(111), Pt(111), Rh(111) and Ru(0001) were determined. For these low coverage structures, the occupation of high symmetry hollow sites by atomic S, notably the fcc site on the (111) surfaces and the hcp site on the (0001) surfaces, fits well into the common trend that S resides on sites with the highest coordination number. For the Re(0001)- c($\sqrt{3} \times 5$)S, both the top and bridge sites are not stable for S adsorption, with the adsorbate relaxing to the neighboring hollow site. For the other phases, the top and bridge sites are not local minima but either a transition state or a higher order saddle point.

Energetic minima were found for various high coverage pure S overlayer structures seen on Pt(111), Rh(111), Re(0001) and Ru(0001) and the calculations provide further information on the structural properties of the systems. The general tendency for mixed site occupation at higher coverages was confirmed. For Ag(111)-($\sqrt{7} \times \sqrt{7}$)S, concern for the validity of structural models proposed in the experimental literature was noted. In the light of the density functional theory results, a refined version of the interacting S trimer model was proposed which consists of an S atom on the top site bonded to two S atoms situated on nearest neighbor off-bridge site positions. Among the different models examined for the Cu(111)-($\sqrt{7} \times \sqrt{7}$)S, the densely packed S-metal overlayer structure proposed by Domangue and Oudar and Prince *et al.*[12,13] was determined to be the most energetically favorable. This model consists of Cu and S atoms in a hexagonal-like arrangement on top of Cu(111), with the S atoms at $\frac{3}{7}$ ML coverage. Theoretical confirmation for the existence of ($5\sqrt{3} \times 2$) clock-like reconstruction on Ni(111) was provided. The Ni overlayer onto which sulfur are adsorbed did not remain in a nearly square unit mesh configuration as in Ni(100), in line with experimental data.

The changes in the surface electronic structure were studied for representative adsorbed systems. It was found that the presence of the adsorbates in the overlayer region broadens the surface *d* band. The dominant mechanism for S interaction with the metal substrate is the overlapping of S *p* and metal *d* bands. At high coverage, noticeable splitting was predicted in the lowest lying S *s* due to enhanced interactions in the overlayer region. Qualitative trends were extracted from Bader charge analysis, such as that S interactions with metals in Ag(111), Cu(111), Ni(111), Re(0001) and Ru(0001) are more ionic than those in Pt(111) and Rh(111).

Supporting Information Available: Figures showing top view of (111) and (0001) surfaces with the adsorption sites indicated. The (2 × 2), (√ 3 × √ 3) and c(√ 3 × 5) unit cells applied in the calculations are also marked. This information is available free of charge via the Internet at http://pubs.acs.org.

FIGURE CAPTIONS

Fig. 1 Binding energies of (a) (2 × 2) phase of S on Ni(111), Pt(111), Re(0001) and Ru(0001) plus c(√ 3 × 5) phase on Re(0001), and (b) (√ 3 × √ 3) phase on Ag(111), Ni(111), Pt(111), Rh(111) and Ru(0001).

Fig. 2 A schematic top view of various relaxed Ag(111)-(√ 7 × √ 7)S. (a) Stable structure according to the model of Schwaha *et al.*, Rovida *et al.* and Heinz *et al.* [8-10] ; (b)-(c) S trimer around top sites of the substrate lattice and (d) S trimer structure proposed in this work. Light blue and yellow spheres represent Ag and S atoms, respectively**.**

Fig. 3 A schematic top view of relaxed Pt(111)-(7 × √ 3)S structures. Blue and yellow spheres represent Pt and S atoms, respectively. Metal atoms labeled Pt_1 and Pt_2 are examples of onefold and twofold S coordinated surface atoms. (a) 1:2 S occupation of the hcp and fcc site position. (b) 1:2 S occupation of the fcc and hcp site position.

Fig. 4 A schematic top view of relaxed high coverage Rh(111) structures. Green and yellow spheres represent Rh and S atoms, respectively. Metal atoms labeled Rh_1, Rh_2 and Rh_3 are examples of onefold, twofold and threefold S coordinated surface atoms. (a) (7 × √ 3) phase, 1:2 S occupation of the hcp and fcc site position. (b) (7 × √ 3) phase, 1:2 S occupation of the fcc and hcp site position. (c) c(4 × 2) phase, 1:1 S occupation of the fcc and hcp site position. (d) (4 × 4) phase, S on the fcc sites

Fig. 5 A schematic top view of relaxed high coverage Re(0001) structures. Blue and yellow spheres represent Re and S atoms, respectively. Metal atoms labeled Re_1, Re_2 and

Re_3 are examples of onefold, twofold and threefold S coordinated surface atoms (a) ($3\sqrt{3} \times 3\sqrt{3}$) phase, S on the hcp sites. (b) $\begin{pmatrix} 3 & 1 \\ 1 & 3 \end{pmatrix}$ phase, S on the hcp sites. (c) ($2\sqrt{3} \times 3\sqrt{2}$) phase, S on the hcp sites.

Fig. 6 A schematic top view of relaxed high coverage Ru(0001) structures. Blue and yellow spheres represent Ru and S atoms, respectively. Metal atoms labeled Ru_1, Ru_2 and Ru_3 are examples of onefold, twofold and threefold S coordinated surface atoms (a) c(4 × 2) phase, 1:1 S occupation of the fcc and hcp site position. (b) ($\sqrt{7} \times \sqrt{7}$) phase: 1:3 S occupation of the fcc and hcp site position.

Fig. 7 Calculated binding energy of S on Ag(111), Pt(111), Rh(111), Re(0001) and Ru(0001) for various phases.

Fig. 8 A schematic top view of various relaxed Cu(111)-($\sqrt{7} \times \sqrt{7}$)-S. Red and yellow spheres represent Cu and S atoms, respectively. (a) Stable structure according to Domangue *et al.* and Prince *et al.*[12,13] Cu_1-Cu_3 refer to Cu overlayer atoms. S on top, hcp and fcc sites are labeled by S_{top}, S_{hcp} and S_{fcc}, respectively. (b) Stable structure according to Foss *et al.*[15,17] Cu_1-Cu_4 refer to Cu overlayer atoms. S on Cu overlayer, hcp and fcc sites are labeled by S_{top}, S_{hcp} and S_{fcc}, respectively (c) Stable geometry from starting structure according to Saidy *et al.*[16] Cu_1-Cu_3 refer to Cu overlayer atoms. S on top of vacancy, hcp site and fcc sites are labeled by S_{vac}, S_{hcp} and S_{fcc}, respectively.

Fig. 9 A schematic top view of low energy Ni(111)-($5\sqrt{3} \times 2$)-S structures.

Fig. 10 The PDOS (E_F =0) for Pt(111)-(2 × 2)S. The two top panels correspond to the PDOS of S and top Pt substrate. The PDOS of the bare surface (bottom panel) is also included.

Fig. 11 Same as in Fig. 11 for Pt(111)-(7 × √ 3)S.

Fig. 12 Same as in Fig. 11 for Cu(111)-(√ 7 × √ 7)S (*Prince* model, Fig 8a). The PDOS of the metal in the overlayer region is also included.

Fig. 13 Total valence population N_e of S obtained from Bader analysis for various ground state low and high coverage S phases. N_e is in unit of $|e|$.

TABLES

Table 1. Predicted adsorption properties of experimentally observed phase of S (low coverage) on various metal surfaces. d(S-M) is the distance between S and surface atoms M, Δ_{12} is percentage change in the first metal-metal interlayer spacing (with respect to the bulk value) and Δz_1 is the magnitude of buckling in the first metal layer.

	E_{bind} (eV/atom)	d(S-M) (Å)	Δz_1 (Å)	Δ_{12} (%)
c(√ 3 × 5) ; θs = ⅕ ML				
Re(0001)				
fcc	-7.41	2.40	0.13	-4.4
hcp	-7.68	2.38	0.09	-4.9
(2 × 2) ; θs = ¼ ML				
Ni(111)				
top	-3.81	2.01	0.24	0.4
bridge	-5.00	2.10	0.14	0.7
hcp	-5.22	2.14	0.08	0.7
fcc	-5.27	2.14 (2.02-2.23 ± 0.02-0.06)[a1] (2.16 ± 0.04)[a2] (2.11 ± 0.03)[a3]	0.05	0.5 (2.7)[i]
Pt(111)				
top	-3.02	2.17	~ 0	0.4
bridge	-4.53	2.24	~ 0	0.2
hcp	-5.03	2.28	0.15	1.8

fcc	-5.23	2.28	0.15	1.8
		(2.24)[b]	(0.08 ± 0.04)[b]	(1.3)[b]
		(2.28 ± 0.03)[c]		
Re(0001)				
top	-4.35	2.13	0.48	-2.5
bridge	-5.36	2.33	0.10	-4.5
fcc	-5.73	2.39	0.15	-3.1
hcp	-5.98	2.38	0.07	-5.1
				(-6.7) [d]
Ru(0001)				
top	-4.12	2.16	~ 0	-4.1
bridge	-5.30	2.29	~ 0	-3.0
fcc	-5.63	2.35	0.03	-3.0
hcp	-5.75	2.33	0.09	-2.1
		(2.29 ± 0.02)[e]	$(0.030^{+0.015}_{-0.030})$[e]	(-1.1) [e]
($\sqrt{3} \times \sqrt{3}$) ; $\theta_S = \frac{1}{3}$ ML				
Ag(111)				
top	-2.68	2.28	0.59	4.6
bridge	-3.54	2.42	0.68	5.1
hcp	-3.62	2.45	0	~ 0
fcc	-3.69	2.45	0	~ 0
Ni(111)				

top	-3.77	2.01	0.41	2.9
bridge	-4.88	2.09	0.45	4.4
hcp	-5.02	2.14	0	1.3
fcc	-5.10	2.14	0	0.9
		(2.13)[f]		
Pt(111)				
top	-2.98	2.17	0.08	0.4
bridge	-4.42	2.24	0.14	2.0
hcp	-4.88	2.28	0	2.5
fcc	-5.04	2.28	0	1.6
		(2.25)[b] (2.28)[c]		(0.4)[b]
Rh(111)				
top	-3.57	2.13	0.09	-2.0
bridge	-5.02	2.22	0.22	1.1
hcp	-5.42	2.27	0	0.6
fcc	-5.50	2.27	0	1.0
		(2.23)[g]		
		(2.25 ± 0.04)[h]		
Ru(0001)				
top	-4.12	2.15	~ 0	-4.0
brg	-5.26	2.28	0.07	-2.5
fcc	-5.68	2.34	0	-2.1
hcp	-5.72	2.33	0	-2.1

	$(2.28 \pm 0.02)^{e}$	$(-0.9)^{e}$

[a1)] Demuth *et al*.[18]; Ohta *et al*. [63]; Warburton *et al.* [25]; Wu *et al.* [19]; Kitajima *et al.* [67]

[a2)] Fauster *et al.* [21]

[a3)] Lüdeke *et al.* [23]

[b)] Yoon *et al*. [31]

[c)] Hayek *et al.* [29]

[d)] Barbieri *et al.* [38]

[e)] Jürgens *et al.* [40]

[f)] Kitajima *et al.* [67]

[g)] Wong *et al.* [35]

[h)] Santoni *et al.* [32]

[i)] Wu *et al.* [77]

Table 2. Predicted adsorption properties of experimentally observed phases of S (high coverage) on various metal surfaces. d(S-M) is the distance between S and surface atoms M, Δ_{12} is percentage change in the first metal-metal interlayer spacing (with respect to the bulk value) and Δz_1 is the magnitude of buckling in the first metal layer. Transition state and higher-order saddle point are denoted as *ts* and *hos*.

	E_{bind} (eV/atom)	d(S-M) (Å)	Δz_1 (Å)	Δ_{12} (%)
Ag(111)				
$(\sqrt{7} \times \sqrt{7})$; $\theta_S = 3/7$ ML				
$S_{top}S_{fcc}S_{hcp}$ (Fig.2a)	-3.18 (*hos*)	2.28 – 2.42	0.68	2.2
S_{3fcc}/S_{3hcp} (Fig.2b-c)	-3.36	2.37 – 2.44	1.10 – 1.14	6.5-6.9
$S_{top}S_{2brg}$ (Fig.2d)	-3.46	2.56 – 2.69	0.20 [a1] ; 0.15 [a2]	-2.0
Pt(111)				
$(7 \times \sqrt{3})$; $\theta_S = 3/7$ ML				
$S_{fcc}S_{2hcp}$ (Fig.3b)	-4.75	2.23 – 2.30	0.33	3.1
$S_{2fcc}S_{hcp}$ (Fig.3a)	-4.80	2.18 – 2.29	0.35	2.5
Rh(111)				
$(7 \times \sqrt{3})$; $\theta_S = 3/7$ ML				
$S_{fcc}S_{2hcp}$ (Fig.4b)	-5.23	2.25 – 2.37	0.24	1.7
$S_{2fcc}S_{hcp}$ (Fig.4a)	-5.24	2.23 – 2.42	0.22	1.6
$c(4 \times 2)$; $\theta_S = 1/2$ ML				
$S_{hcp}S_{top}$	-4.28 (*hos*)	2.14-2.28	0.05	1.0

$S_{fcc}S_{top}$	-4.29 (*hos*)	2.14-2.28	~ 0	0.9
$S_{fcc}S_{hcp}$ (Fig.4c)	-5.11	2.23 - 2.28	0.24	2.7
(4×4); $\theta_S = \frac{1}{2}$ ML				
S_{hcp}	-4.93	2.20 – 2.35	0.50 [b1] ; 0.22 [b2]	4.4
S_{fcc} (Fig. 4d)	-4.93	2.21 – 2.37	0.38 [b1] ; 0.23 [b2]	3.5
Re(0001)				
$(3\sqrt{3} \times 3\sqrt{3})$; $\theta_S = \frac{4}{9}$ ML				
S_{fcc}	-5.46	2.33-2.48	0.11 [b1] ; 0.26 [b2]	-2.9
S_{hcp} (Fig.5a)	-5.72	2.35-2.43	0.11 [b1] ; 0.17 [b2]	-3.2
$\begin{pmatrix} 3 & 1 \\ 1 & 3 \end{pmatrix}$; $\theta_S = \frac{1}{2}$ ML				
S_{fcc}	-5.42	2.35-2.44	0.22 [b1] ; 0.25 [b2]	-1.8
S_{hcp} (Fig.5b)	-5.67	2.35 – 2.44	0.15 [b1] ; 0.16 [b2]	-2.4
$(2\sqrt{3} \times 2\sqrt{3})$; $\theta_S = \frac{1}{2}$ ML				
S_{fcc}	-5.35	2.34 – 2.43	0.14-0.31 [b2]	-1.9
S_{hcp} (Fig.5c)	-5.65	2.34 – 2.43	0.13-0.21 [b2]	-2.0
		(2.34 – 2.51) [r1]		(-0.9) [r1]
Ru(0001)				
$c(4 \times 2)$; $\theta_S = \frac{1}{2}$ ML				
$S_{hcp}S_{top}$	-4.49 (*ts*)	2.15-2.35	0.09	0.9
$S_{fcc}S_{top}$	-4.56 (*ts*)	2.14-2.33	0.09	-1.6
$S_{hcp}S_{fcc}$ (Fig.6a)	-5.44	2.27 – 2.33	0.21	0.1

		(2.24 – 2.29) [r2]	(0.19 ± 0.02) [r2]	(0.5) [r2]
($\sqrt{7} \times \sqrt{7}$); $\theta_S = 4/7$ ML				
$S_{3fcc}S_{hcp}$	-5.25	2.27 – 2.36	0.34 [b1]; 0.17 [b2]	2.0
$S_{3hcp}S_{fcc}$ (Fig.6b)	-5.28	2.26 – 2.35	0.42 [b1]; 0.20 [b2]	2.1
		(2.23-2.33 ± 0.05)[r3]	(0.39 ± 0.02) [b1,r3]	(1.4) [r3]
			(0.18 ± 0.02) [b2,r3]	

[a1)] buckling between Ag bonded to S_{top} and Ag bonded to S_{brg}

[a2)] buckling between Ag bonded to S_{brg} and the remaining under coordinated Ag

[b1)] buckling between three-fold and two-fold S coordinated metal atoms

[b2)] buckling between two-fold and one-fold S coordinated metal atoms

[r1)] Barbieri *et al*. [38]

[r2)] Schwennicke *et al.* [44]

[r3)] Sklarek *et al.* [43]

Table 3. E_{bind}', for the various examined Cu(111)-($\sqrt{7} \times \sqrt{7}$)-S models. Relevant structural properties for the most stable case are tabulated. $d(S_i\text{-Cu})$ is the distance between S on the i site and Cu overlayer. The various $\Delta z_1(S_i\text{-Cu})$ refer to the magnitude of buckling between S on the i site and the top Cu substrate center of mass.

	E_{bind}' (eV)	
Foss (Fig. 8b)	-13.10	
Saidy (Fig. 8c)	-11.90	
Prince (Fig. 8a)	-13.21	
	Structural properties	
	$d(S_{top}\text{-Cu})$ (Å)	2.22
	$d(S_{hcp}\text{-Cu})$ (Å)	2.37
	$d(S_{fcc}\text{-Cu})$ (Å)	2.27
	$\Delta z_1(S_{top}\text{-Cu})$ (Å	2.52, (2.30) [a]
	$\Delta z_1(S_{hcp}\text{-Cu})$ (Å)	2 .05, (1.77) [a]
	$\Delta z_1(S_{fcc}\text{-Cu})$ (Å)	1.91, (1.77) [a]

[a] Prince *et al*. [13]

Table 4. Adsorption energy, E_{bind}', per surface unit cell and structural properties of the low energy Ni(111)-(5√ 3 × 2)S structures obtained in this work.

	C_1 (Fig. 9a)	C_2 (Fig. 9b)
E_{bind}' (eV)	-42.09	-42.06
d($Ni_{overlayer}$-$Ni_{substrate}$) (Å) [a]	2.40 − 2.72	2.39 − 2.73
d($Ni_{overlayer}$-$Ni_{overlayer}$) (Å) [b]	2.48 − 2.67	2.47-2.67
d(S-$Ni_{overlayer}$) (Å) [c]	2.15 − 2.20	2.15 − 2.21
d(S-$Ni_{substrate}$) (Å) [d]	2.27	2.27
Δz_1 (S-$Ni_{overlayer}$) (Å) [e]	3.25, (3.28 ± 0.1)[g]	3.25
Δz_1'(S-$Ni_{overlayer}$) (Å) [f]	2.49, (2.48 ± 0.1)[g]	2.46

[a] bondlengths between overlayer Ni and top layer Ni substrate

[b] bondlengths between overlayer Ni

[c] bondlengths between S and overlayer Ni

[d] bondlengths between S and the top layer Ni substrate

[e] vertical distance between upper S adatoms center of mass and top Ni substrate center of mass

[f] vertical distance between lower S adatoms center of mass and top Ni substrate center of mass

[g] Lüdeke *et al.* [23]

Fig. 1

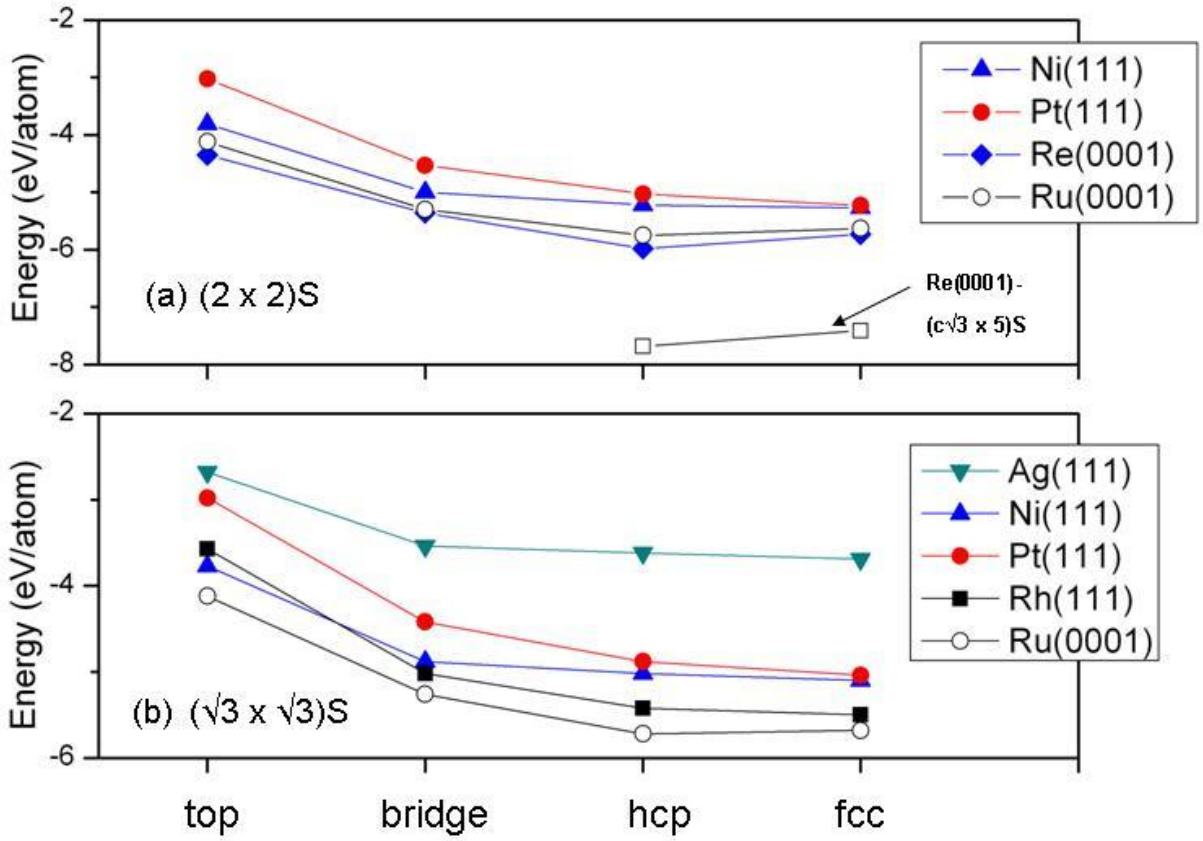
Energy (eV/atom)
-2
-4
-6
-8
(a) (2 x 2)S
Ni(111)
Pt(111)
Re(0001)
Ru(0001)
Re(0001)-
(c√3 x 5)S
Energy (eV/atom)
-2
-4
-6
(b) (√3 x √3)S
Ag(111)
Ni(111)
Pt(111)
Rh(111)
Ru(0001)
top
bridge
hcp
fcc

Fig. 2

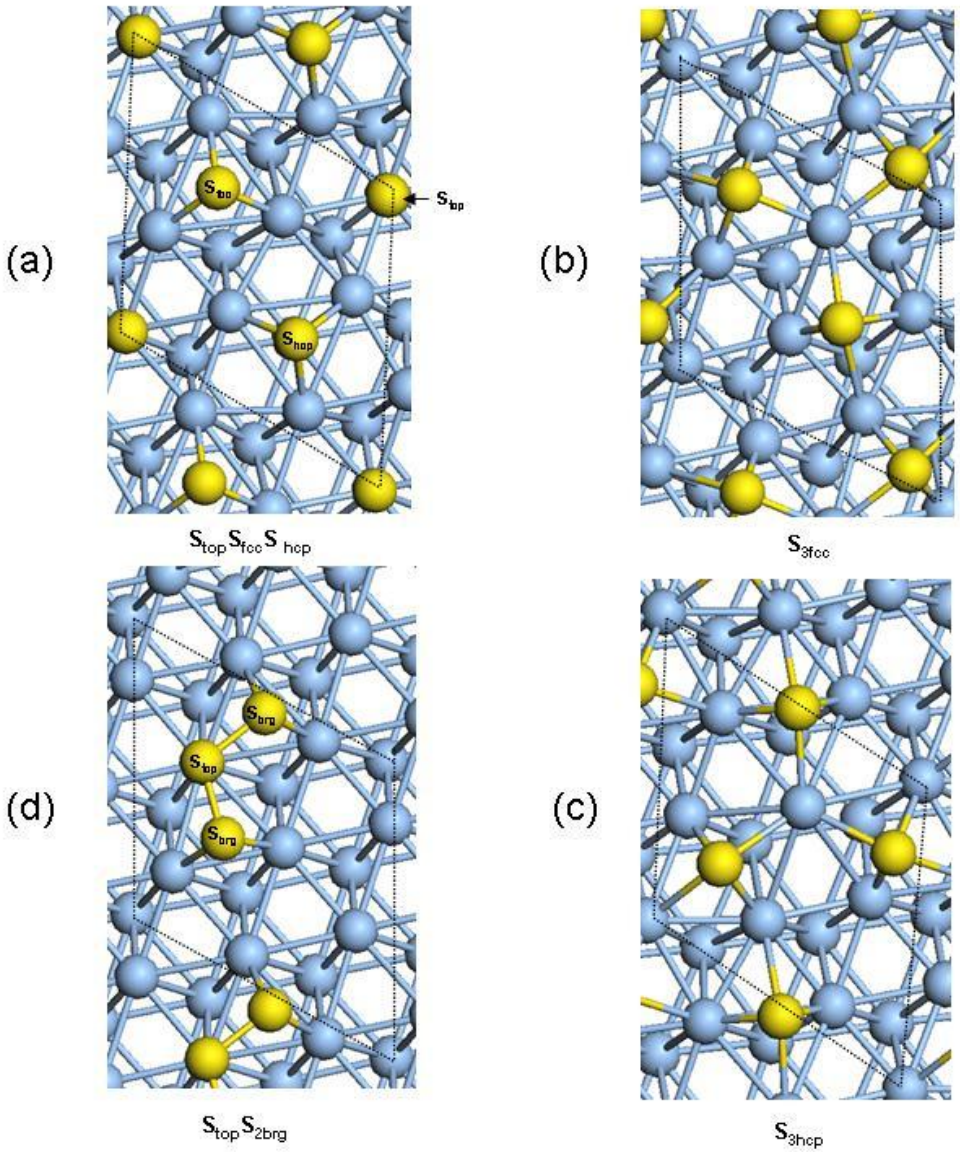
(a)
S_{fcc}
S_{top}
S_{hcp}
$S_{top}S_{fcc}S_{hcp}$
(b)
S_{3fcc}
(d)
S_{brg}
S_{top}
S_{brg}
$S_{top}S_{2brg}$
(c)
S_{3hcp}

Fig. 3

(a)

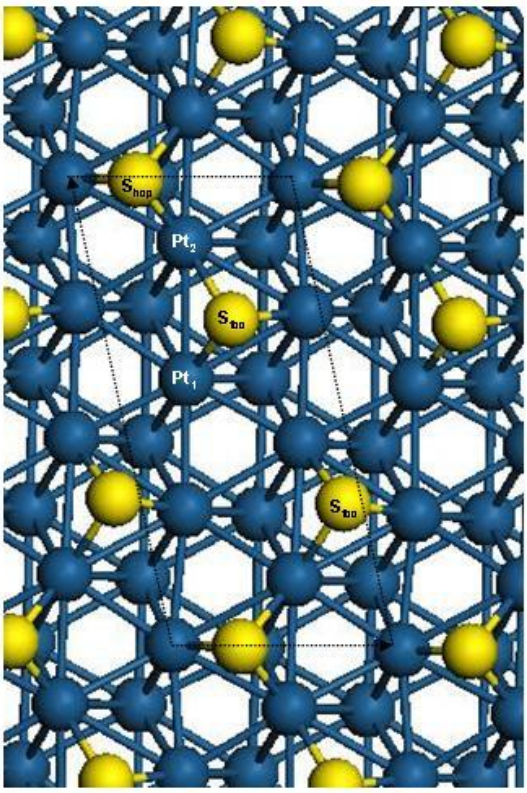

$S_{2fcc}S_{hcp}$

(b)

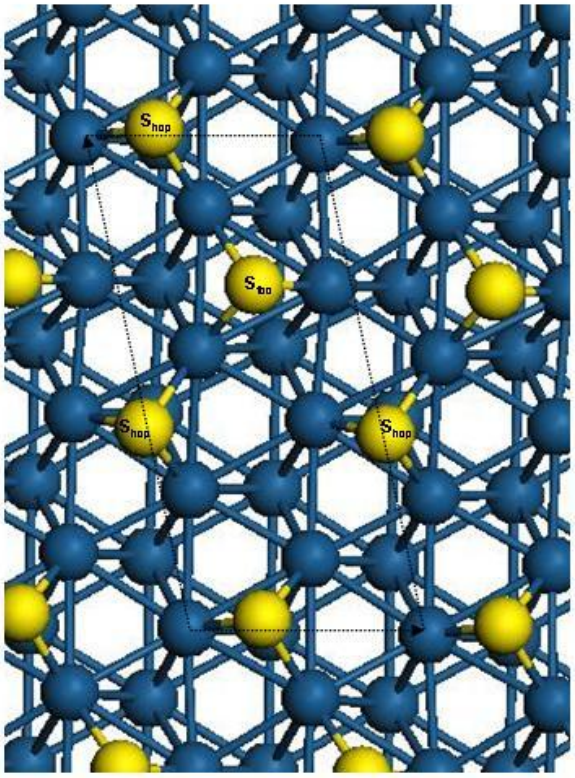

$S_{2hcp}S_{fcc}$

Fig. 4

(a)

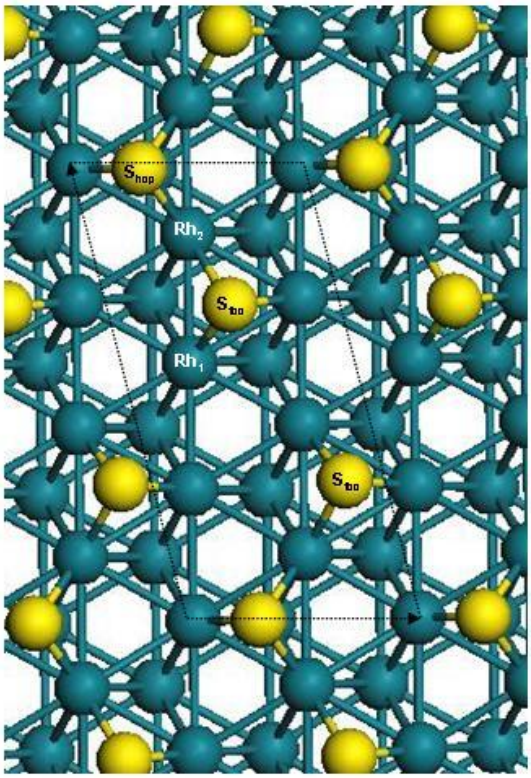

$S_{2fcc}S_{hcp}$

(b)

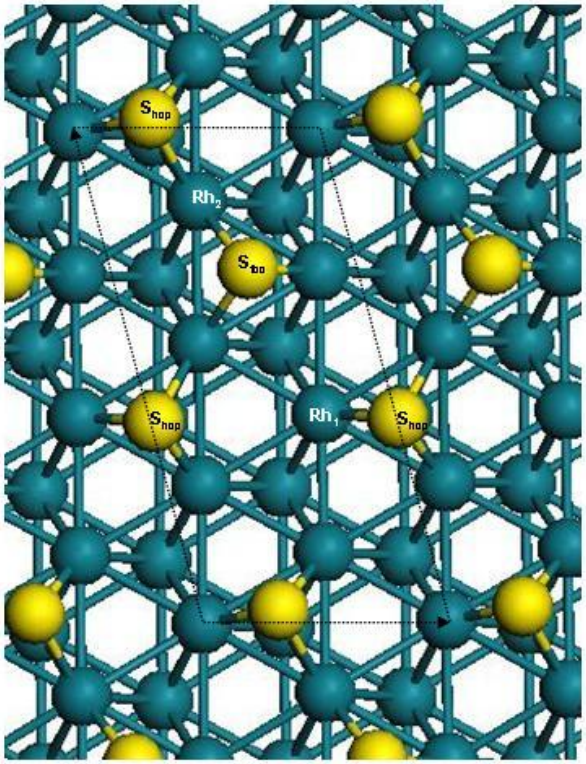

$S_{2hcp}S_{fcc}$

Fig. 4

(c)

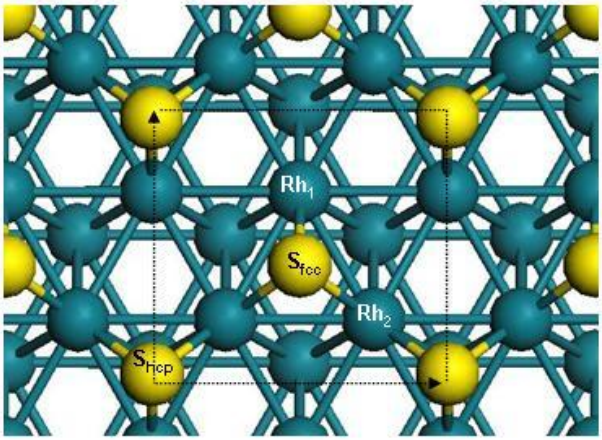

$S_{fcc}S_{hcp}$

(d)

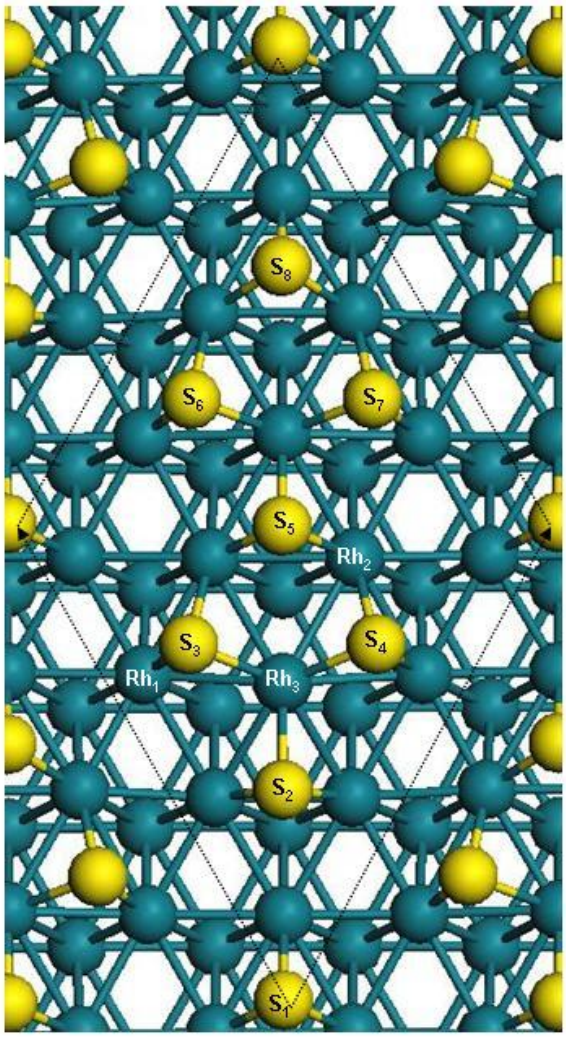

S_{fcc}

Fig. 5a

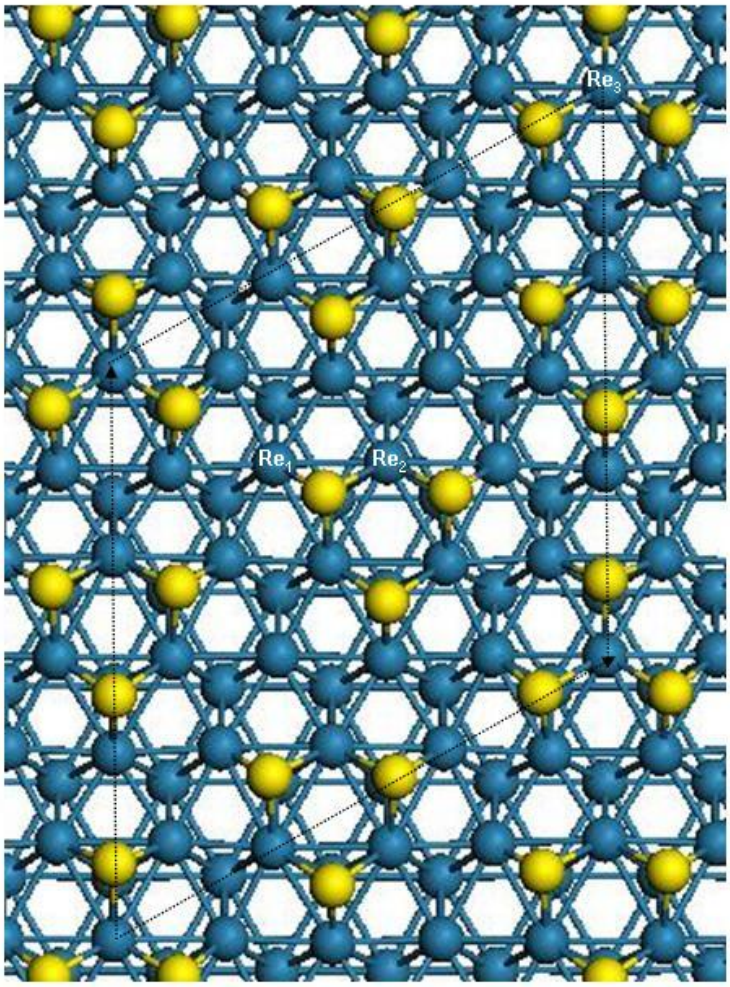

S_{hcp}

Fig. 5b

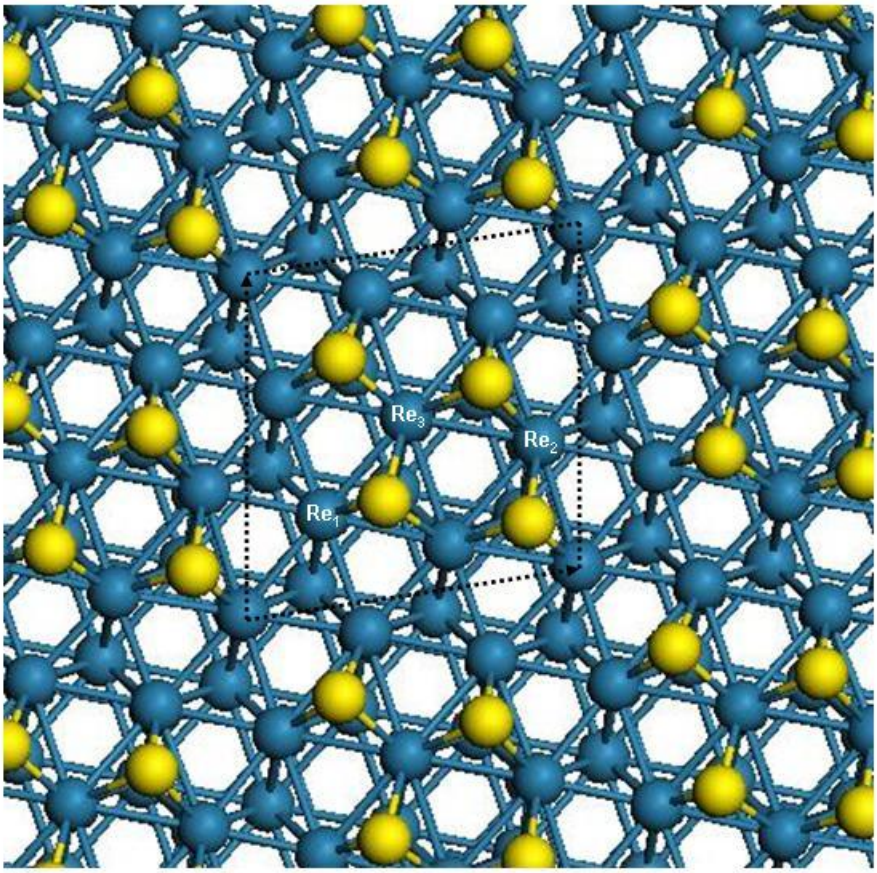

S_{hcp}

Fig. 5c

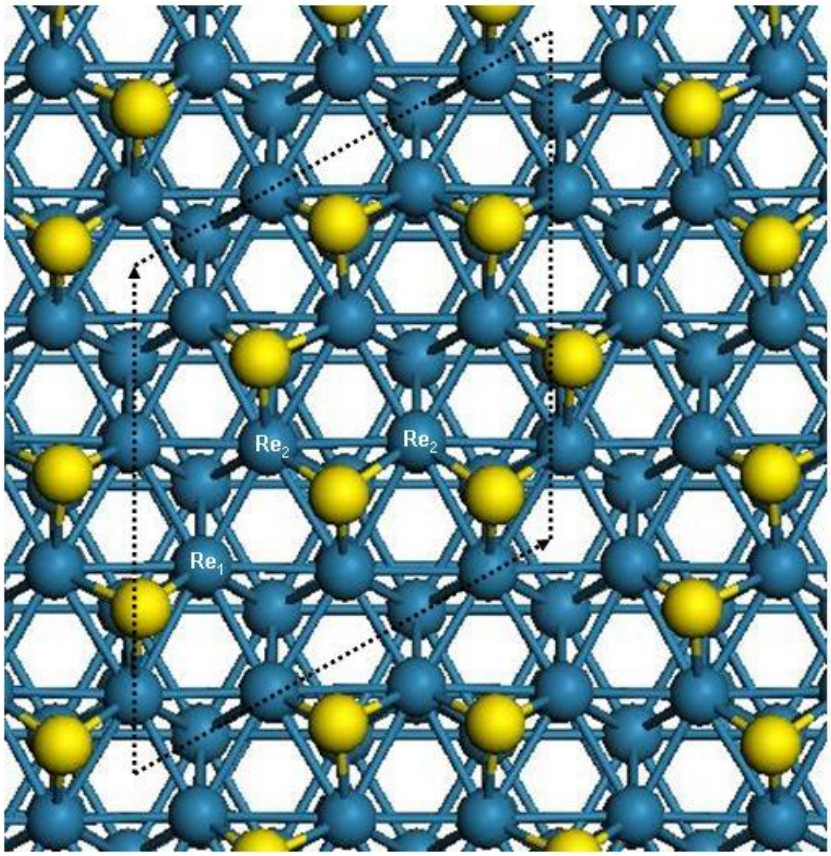

S_{hcp}

Fig. 6

(a)

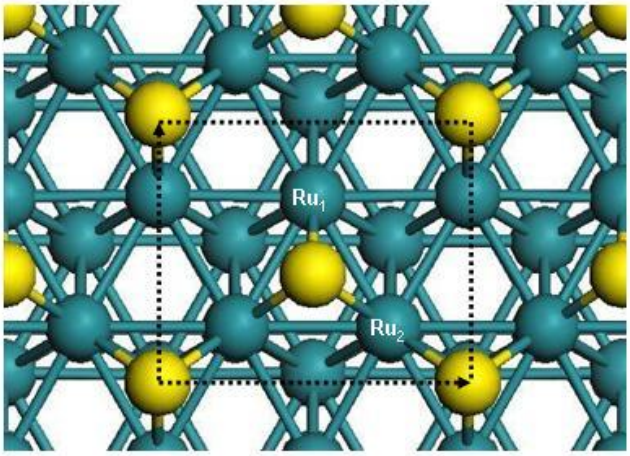

$S_{fcc}S_{hcp}$

(b)

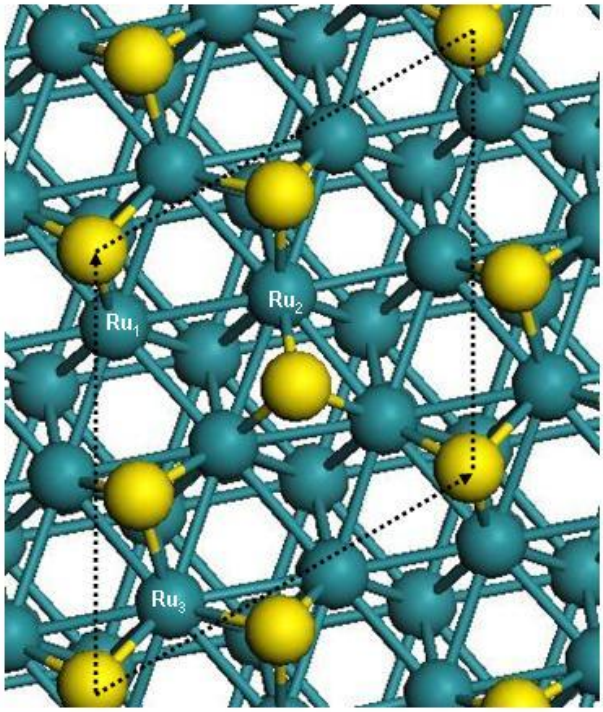

$S_{3hcp}S_{fcc}$

Fig. 7

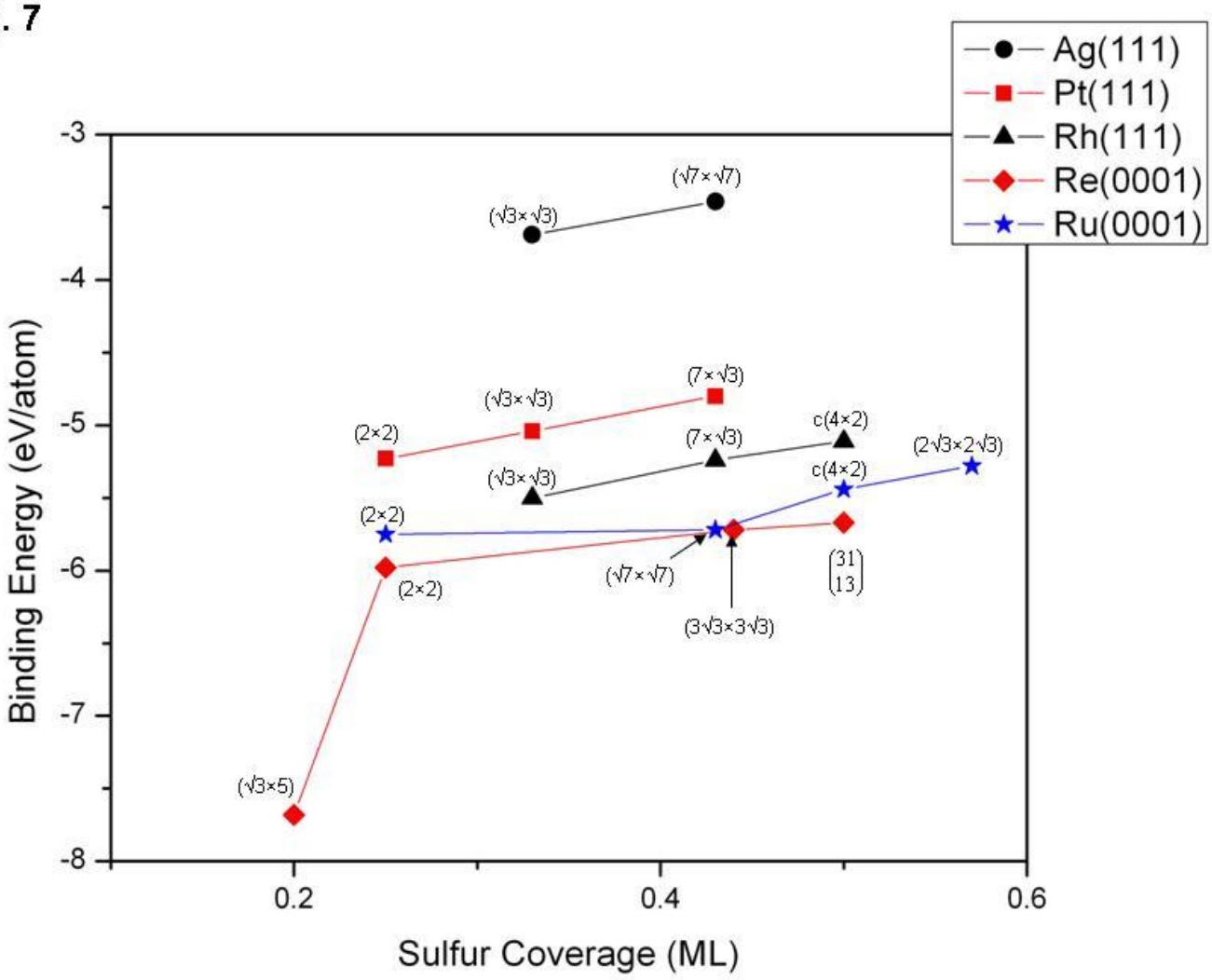
Ag(111)
Pt(111)
Rh(111)
Re(0001)
Ru(0001)
Binding Energy (eV/atom)
Sulfur Coverage (ML)
-3
-4
-5
-6
-7
-8
0.2
0.4
0.6
(√7×√7)
(√3×√3)
(7×√3)
(√3×√3)
c(4×2)
(2×2)
(7×√3)
(√3×√3)
c(4×2)
(2√3×2√3)
(2×2)
(2×2)
(√7×√7)
(31 13)
(3√3×3√3)
(√3×5)

Fig. 8a

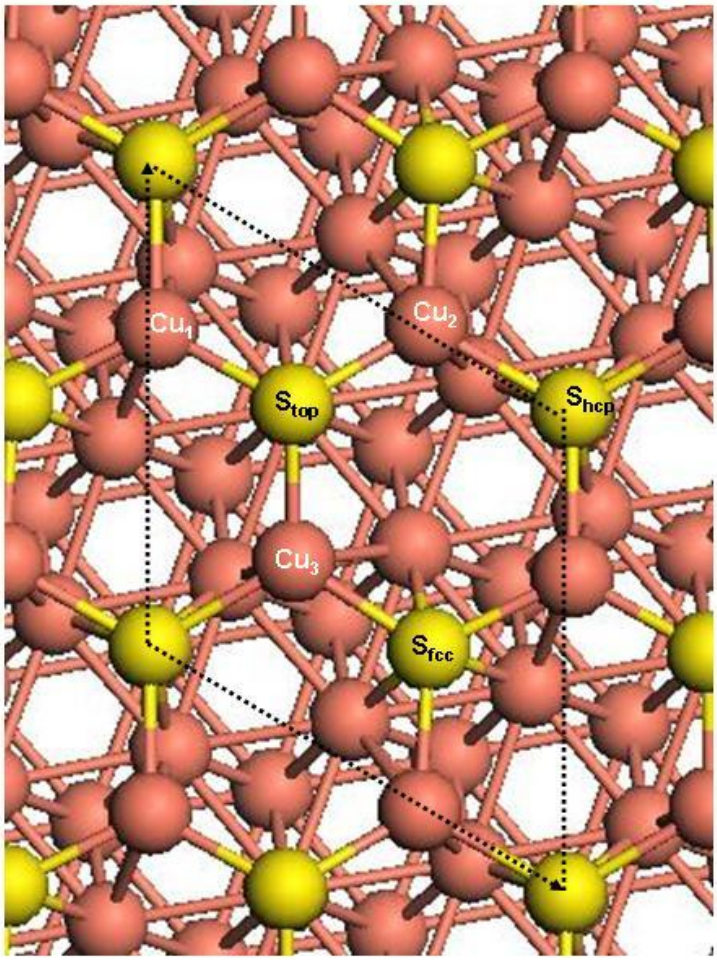

Prince

Fig. 8b

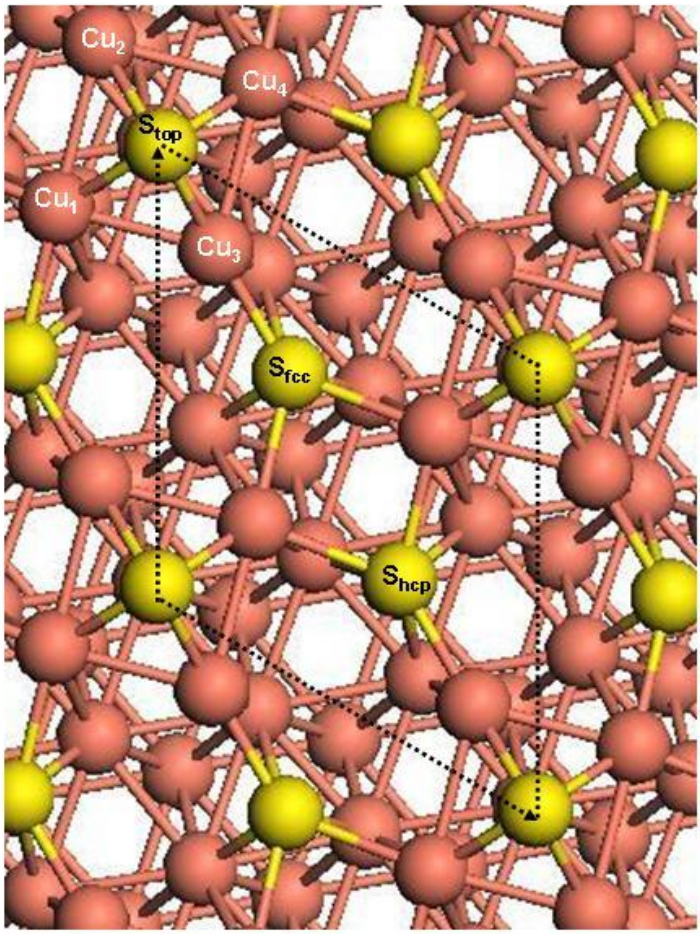

Foss

Fig. 8c

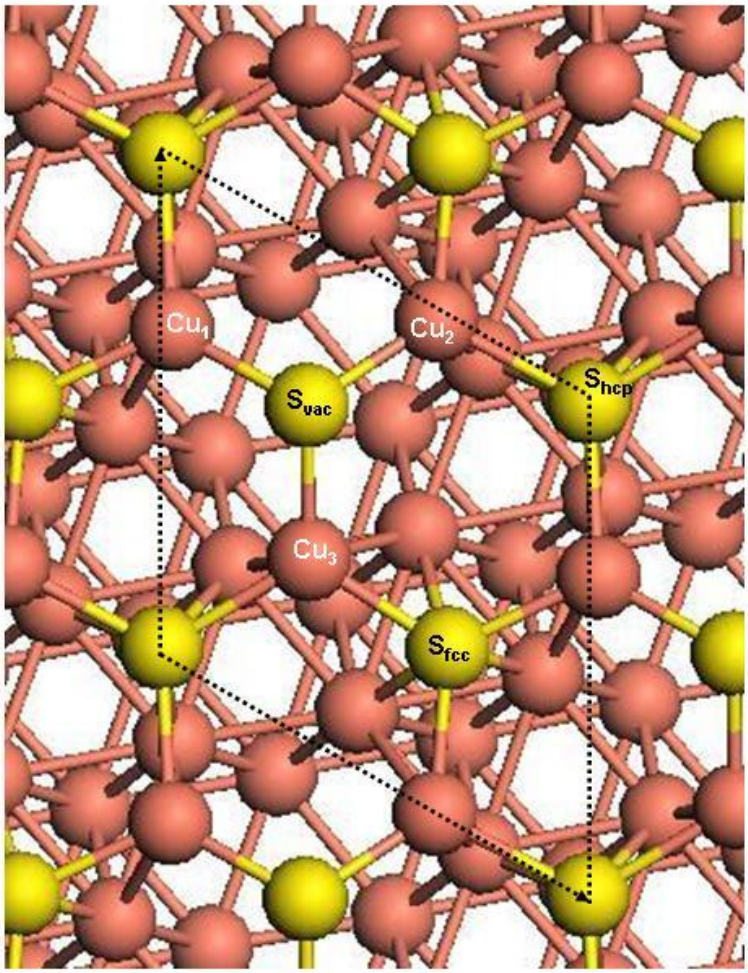

Saidy

Fig. 9a

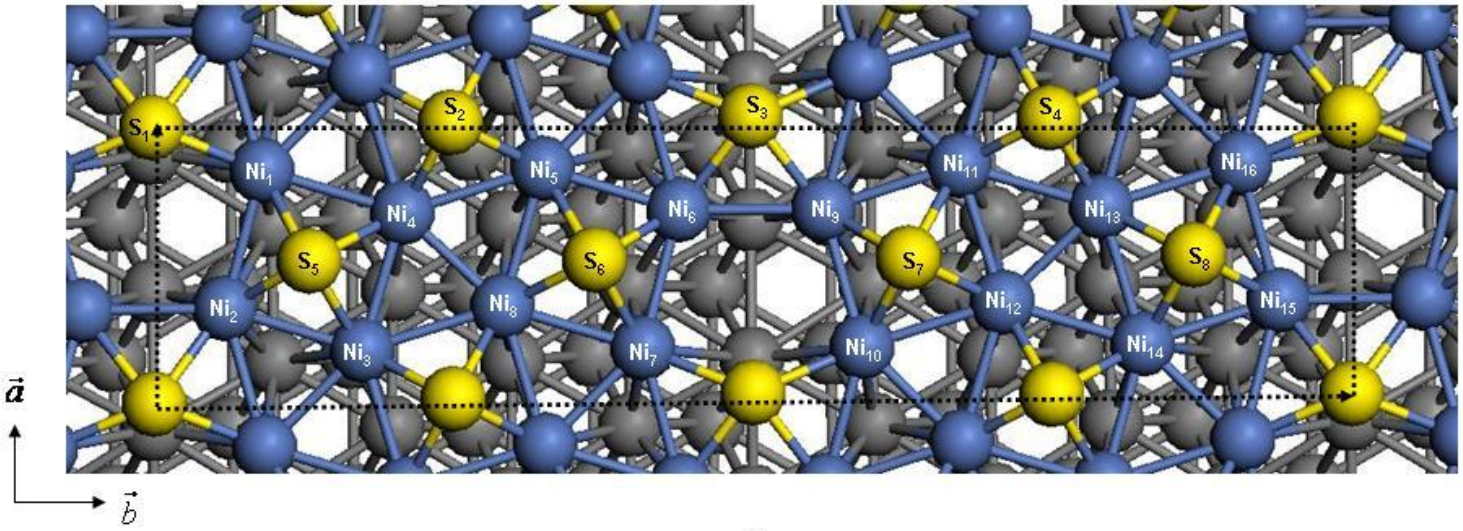
S1
S2
S3
S4
Ni1
Ni5
Ni11
Ni16
Ni4
Ni6
Ni9
Ni13
S5
S6
S7
S8
Ni2
Ni8
Ni12
Ni15
Ni3
Ni7
Ni10
Ni14
a
b

C_1

Fig. 9b

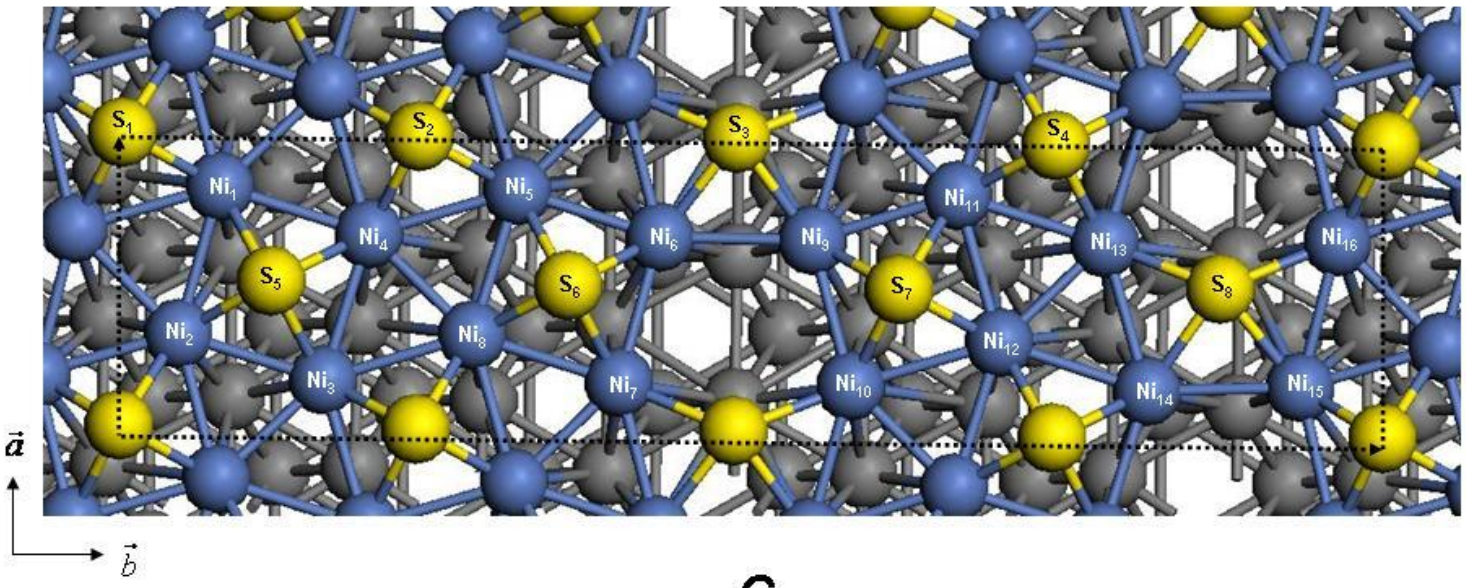
S1
S2
S3
S4
Ni1
Ni5
Ni11
Ni4
Ni6
Ni9
Ni13
Ni16
S5
S6
S7
S8
Ni2
Ni8
Ni12
Ni3
Ni7
Ni10
Ni14
Ni15
$\vec{a}$
$\vec{b}$

C_2

Fig. 10

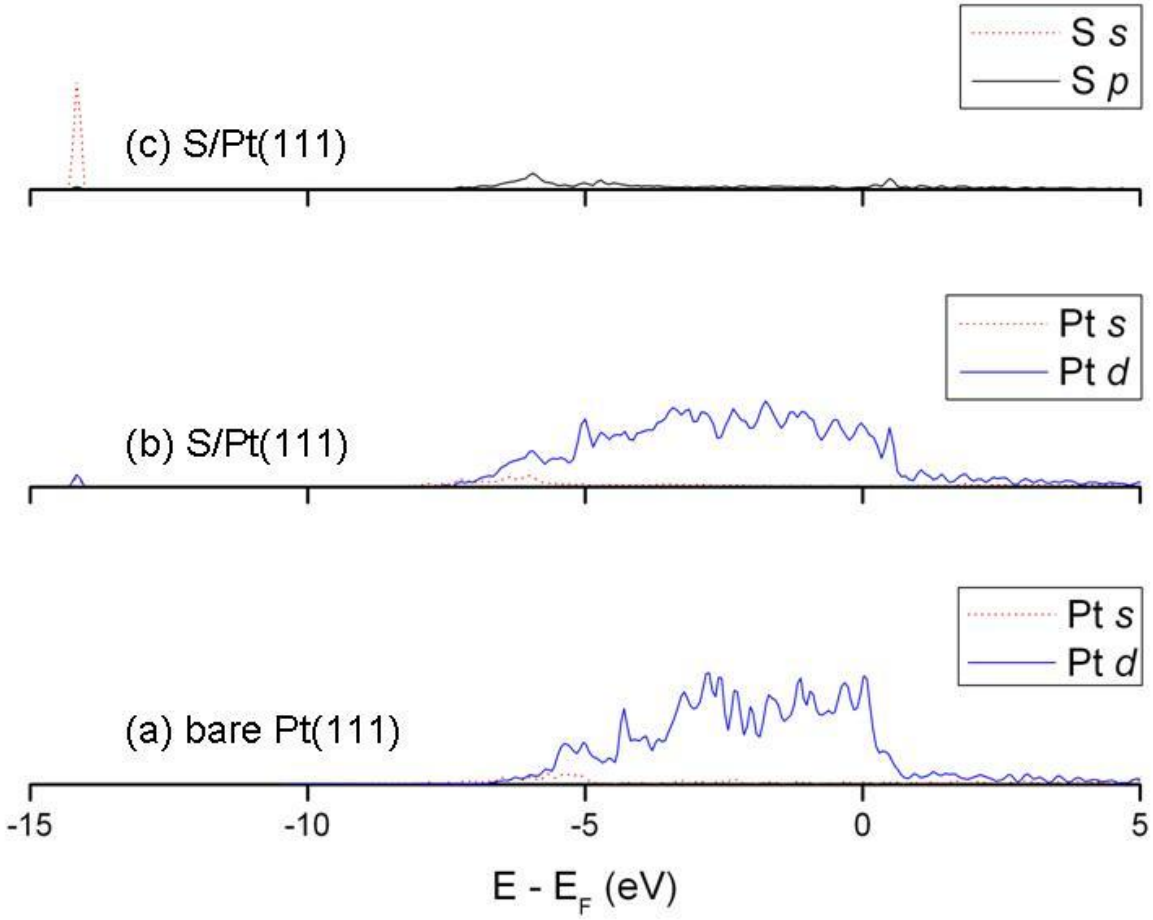
S s
S p
(c) S/Pt(111)
Pt s
Pt d
(b) S/Pt(111)
Pt s
Pt d
(a) bare Pt(111)
-15
-10
-5
0
5
E - E_F (eV)

Fig. 11

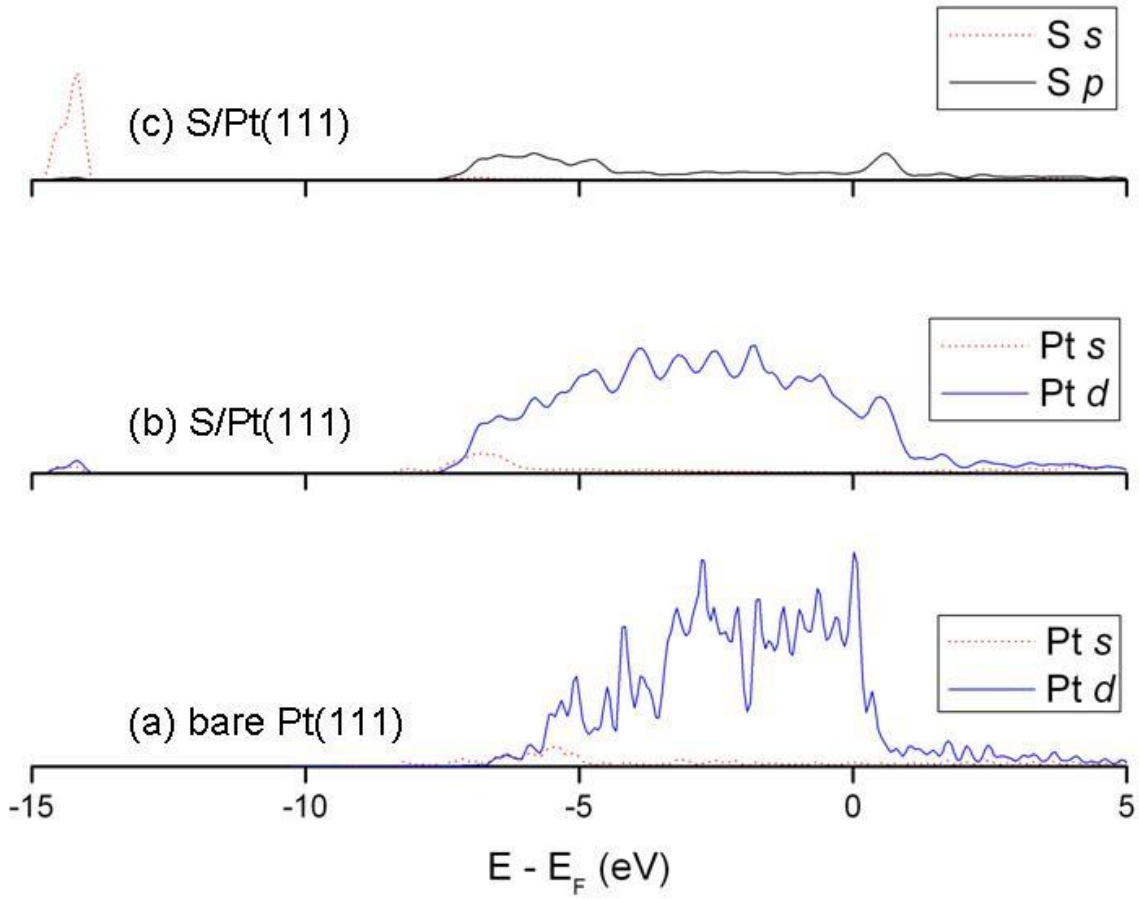
S s
S p
(c) S/Pt(111)
Pt s
Pt d
(b) S/Pt(111)
Pt s
Pt d
(a) bare Pt(111)
-15
-10
-5
0
5
E - E_F (eV)

Fig. 12

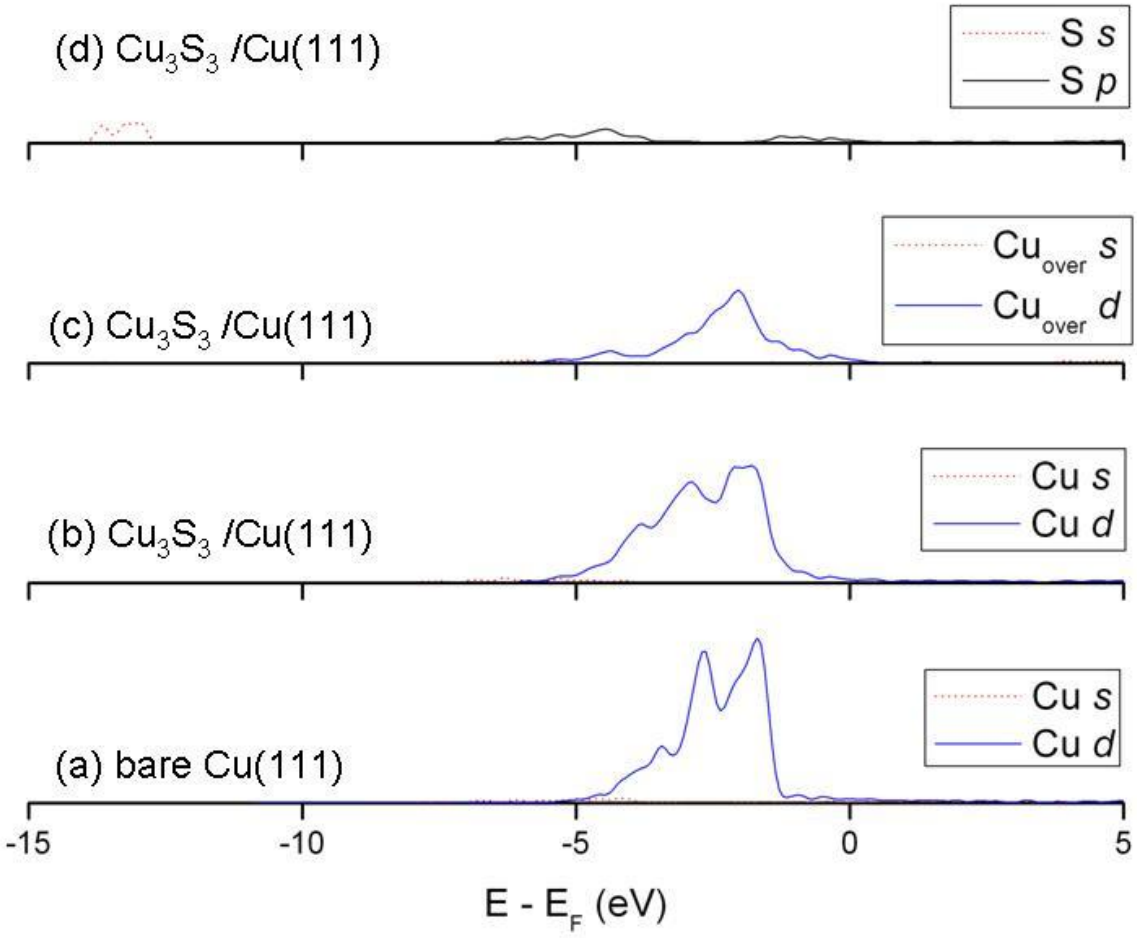
(d) Cu3S3 /Cu(111)
S s
S p
(c) Cu3S3 /Cu(111)
Cu over s
Cu over d
(b) Cu3S3 /Cu(111)
Cu s
Cu d
(a) bare Cu(111)
Cu s
Cu d
-15
-10
-5
0
5
E - EF (eV)

Fig. 13

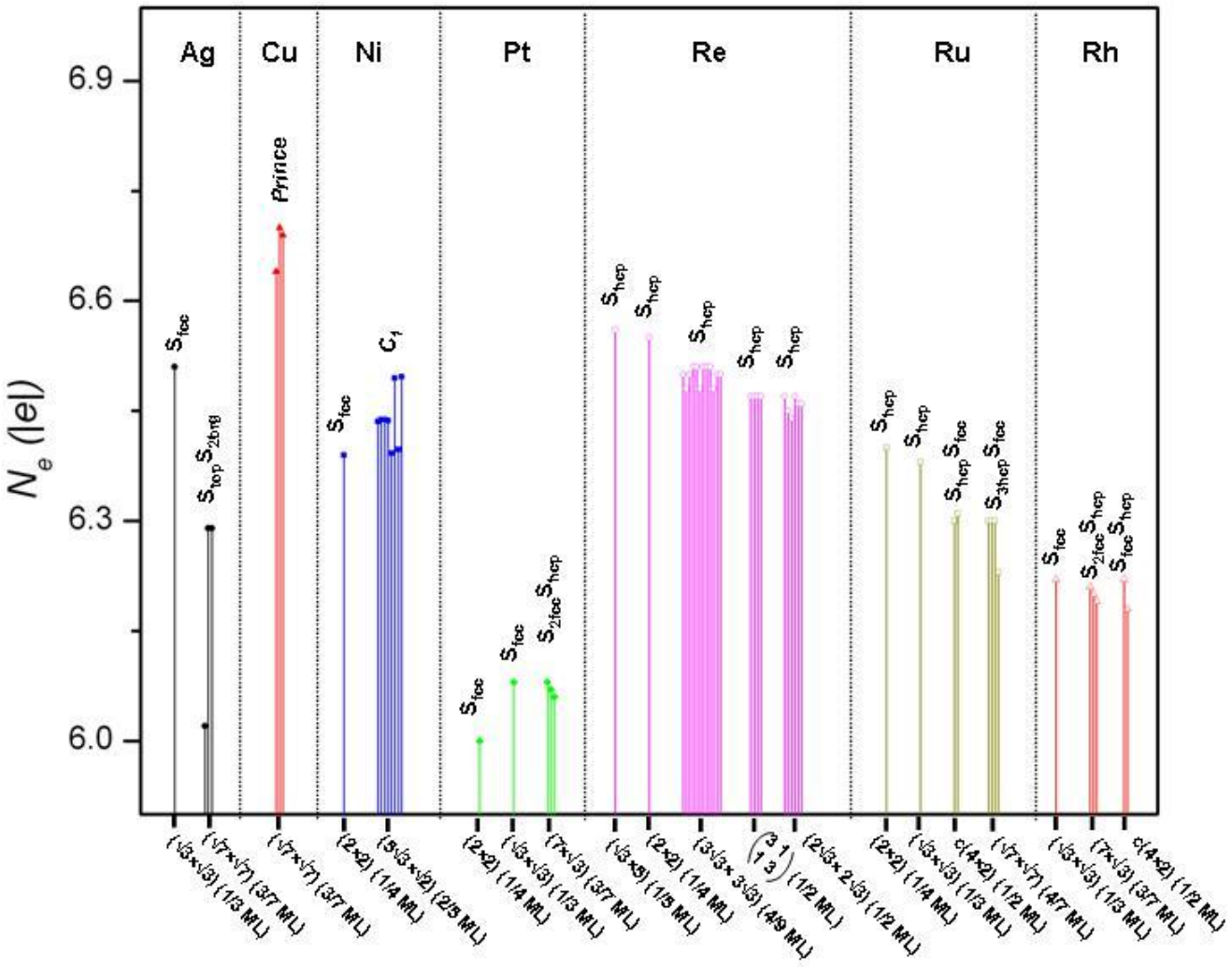
Ag
Cu
Ni
Pt
Re
Ru
Rh
N_e (|e|)
6.9
6.6
6.3
6.0
Prince
S_{fcc}
S_{top}
S_{2trig}
C_1
S_{hcp}
S_{2fcc}
S_{3hcp}
S_{2hcp}
S_{3fcc}
(√3×√3) (1/3 ML)
(√7×√7) (3/7 ML)
(√7×√7) (3/7 ML)
(2×2) (1/4 ML)
(5√3×√2) (2/5 ML)
(2×2) (1/4 ML)
(√3×√3) (1/3 ML)
(7×√3) (3/7 ML)
(√3×5) (1/5 ML)
(2×2) (1/4 ML)
(3√3× 3√3) (4/9 ML)
(1/2 ML)
(2√3× 2√3) (1/2 ML)
(2×2) (1/4 ML)
(√3×√3) (1/3 ML)
c(4×2) (1/2 ML)
(√7×√7) (1/2 ML)
(√3×√3) (1/3 ML)
(7×√3) (3/7 ML)
c(4×2) (1/2 ML)

References

(1) Bartholomew, C. H.; Agrawal, P. K.; Katzer, J. R. *Adv. Catal.* 1982, *31*, 135.

(2) Goodman, D. W. *Appl. Surf. Sci.* 1984, *19*, 1.

(3) Campbell, C. T.; Koel, B. E. *Surf. Sci.* 1987, *183*, 100.

(4) Rodriguez, J. A.; Hrbek, J. *Acc. Chem. Res.* 1999, *32*, 719.

(5) Rodriguez, J. A. *Prog. Surf. Sci.* 2006, *81*, 141.

(6) Roa, F.; Way, J. D.; McCormick, R. L.; Paglieri, S. N. *Chem. Eng. J.* 2003, *93*, 11.

(7) Adhikari, S.; Fernando, S. *Ind. Eng. Chem. Res.* 2006, *45*, 875.

(8) Schwaha, K.; Spencer, N. D.; Lambert, R. M. *Surf. Sci.* 1979, *81*, 273.

(9) Rovida, G.; Pratesi, F. *Surf. Sci.* 1981, *104*, 609.

(10) Heinz, R.; Rabe, J. P. *Langmuir* 1995, *11*, 506.

(11) Aloisi, G. D.; Cavallini, M.; Innocenti, M.; Foresti, L.; Pezzatini, G.; Guidelli, R. *J. Phys. Chem. B* 1997, *101*, 4774.

(12) Domange, J. L.; Oudar, J. *Surf. Sci.* 1968, *11*, 125.

(13) Prince, N. P.; Seymour, D. L.; Ashwin, M. J.; McConville, C. F.; Woodruff, D. P.; Jones, R. G. *Surf. Sci.* 1990, *230*, 13.

(14) Kitajima, Y.; Takata, Y.; Sato, H.; Yokohama, T.; Ohta, T.; Kuroda, H. *Jpn. J. Appl. Phys.* 1993, *32*, 377.

(15) Foss, M.; Feidenhans'l, R.; Nielsen, M.; Findeisen, E.; Buslaps, T.; Johnson, R. L.; Besenbacher, F. *Surf. Sci.* 1997, *388*, 5.

(16) Saidy, M.; Mitchell, K. A. R. *Surf. Sci.* 1999, *441*, 425.

(17) Jackson, G. J.; Driver, S. M.; Woodruff, D. P.; Cowie, B. C. C.; Jones, R. G. *Surf. Sci.* 2000, *453*, 183.

(18) Demuth, J. E.; Jepsen, D. W.; Marcus, P. *Phys. Rev. Lett.* 1974, *32*, 1182.

(19) Wu, Y. K.; Mitchell, K. A. R. *Can. J. Chem. Eng.* 1989, *67*, 1975.

(20) Capehart, T. W.; Rhodin, T. N. *J. Vac. Sci. Technol.* 1979, *16*, 594.

(21) Fauster, T.; Durr, H.; Hartwig, D. 1986, *178*, 657.

(22) Ku, Y.; Overbury, S. H. *Surf. Sci.* 1992, *276*, 262.

(23) Lüdeke, J.; Ettema, A. R. H. F.; Driver, S. M.; Scragg, G.; Kerkar, M.; Woodruff, D. P.; Cowie, B. C. C.; Jones, R. G.; Bastow, S. *Surf. Sci.* 1996, *366*, 260.

(24) Edmonds, T.; McCarroll, J. J.; Pitkethly, R. C. *J. Vac. Sci. Technol.* 1971, *8*, 68.

(25) Warburton, D. R.; Wincott, P. L.; Thornton, G.; Quinn, F. M.; Norman, D. *Surf. Sci.* 1989, *211/212*, 71.

(26) Kitama, Y.; Yokoyama, T.; Obta, T.; Funabashi, M.; Kosugi, N.; Kuroda, H. *Surf. Sci.* 1989, *214*, L261.

(27) Perdereau, M.; Oudar, J. *Surf. Sci.* 1970, *20*, 80.

(28) Heegemann, W.; Meister, K. H.; Bechtold, E.; Hayek, K. *Surf. Sci.* 1975, *49*, 161.

(29) Hayek, K.; Glassl, H.; Gutmann, A.; Leonhard, H.; Prutton, M.; Tear, S. P.; Welton-Cook, M. R. *Surf. Sci.* 1985, *152/153*, 419.

(30) Hayek, K.; Glassl, H.; Gutmann, A.; Leonhard, H.; Prutton, M.; Tear, S. P.; Welton-Cook, M. R. *Surf. Sci.* 1986, *175*, 535.

(31) Yoon, H. A.; Materer, N.; Salmeron, M.; Hove, M. A. V.; Somorjai, G. A. *Surf. Sci.* 1997, *376*, 254.

(32) Santoni, A.; Cowie, B. C. C.; Scarel, G.; Dhanak, V. R. *Surf. Sci.* 1997, *388*, 254.

(33) Foord, J. S.; Reynolds, A. E. *Surf. Sci.* 1985, *164*, 640.

(34) Yoon, H. A.; Salmeron, M.; Somorjai, G. A. *Surf. Sci.* 1998, *395*, 268.

(35) Wong, K. C.; Liu, W.; Saidy, M.; Mitchell, K. A. R. *Surf. Sci.* 1996, *345*, 101.

(36) Ogletree, D. F.; Hwang, R. Q.; Zeglinski, D. M.; Lopez Vazquez-de-Parga, A.; Somorjai, G. A.; Salmeron, M. *J. Vac. Sci. Technol. B* 1991, *9*, 886.

(37) Sautet, P.; Dunphy, J. C.; Ogletree, D. F.; Joachim, C.; Salmeron, M. *Surf. Sci.* 1994, *315*, 127.

(38) Barbieri, A.; Jentz, D.; Materer, N.; Held, G.; Dunphy, J. C.; Ogletree, D. F.; Sautet, P.; Salmeron, M.; Van Hove, M. A.; Somorjai, G. A. *Surf. Sci.* 1994, *312*, 10.

(39) Hwang, R. Q.; Zeglinski, D. M.; Lopez Vazquez-de-Parga, A.; Ogletree, D. F.; Somorjai, G. A.; Salmeron, M. *Phys. Rev. B* 1991, *44*, 1914.

(40) Jürgens, D.; Held, G.; Pfnür, H. *Surf. Sci.* 1994, *303*, 77.

(41) Jürgens, D.; Schwennicke, C.; Pfnür, H. *Surf. Sci.* 1997, *381*, 174.

(42) Müller, T.; Heuer, D.; Pfnür, H.; Köhler, U. *Surf. Sci.* 1996, *347*, 80.

(43) Sklarek, W.; Schwennicke, C.; Jürgens, D.; Pfnür, H. *Surf. Sci.* 1995, *330*, 11.

(44) Schwennicke, C.; Jürgens, D.; Held, G.; Pfnür, H. *Surf. Sci.* 1994, *316*, 81.

(45) Wahlström, E.; Ekvall, I.; Kihlgren, T.; Olin, H.; Lingren, S.; Walldén, L. *Phys. Rev. B* 2001, *64*, 155406.

(46) Foss, M.; Feidenhans'l, R.; M., N.; Findeisen, E.; Johnson, R. L.; Buslaps, T.; Stensgaard, I.; Besenbacher, F. *Phys. Rev. B* 1994, *50*, 8950.

(47) Mullins, D. R.; Huntley, D. R.; Overbury, S. H. *Surf. Sci.* 1995, *323*, L287.

(48) Alfonso, D. R.; Cugini, A. V.; Sholl, D. S. *Surf. Sci.* 2003, *546*, 12.

(49) Albenze, E. J.; Shamsi, A. *Surf. Sci.* 2006, *600*, 3202.

(50) Yang, Z.; Wu, R.; Rodriguez, J. A. *Phys. Rev. B* 2002, *65*, 155409.

(51) Michaelides, A.; Hu, P. *J. Chem. Phys.* 2001, *115*, 8570.

(52) Zhang, C. J.; Hu, P.; Lee, M.-H. *Surf. Sci.* 1999, *432*, 305.

(53) Mavrikakis, M.; Rempel, J.; Greeley, J.; Hansen, L. B.; Nørskov, J. K. *J. Chem. Phys.* 2002, *117*, 6737.

(54) Alfonso, D. *Surf. Sci.* 2007, *601*, 4899.

(55) Kresse, G.; Hafner, J. *Phys. Rev. B* 1994, *49*, 14251.

(56) Kresse, G.; Fürthmuller, J. *Phys. Rev. B* 1996, *54*, 11169.

(57) Perdew, J. P.; Burke, K.; Enzerhof, M. *Phys. Rev. Lett.* 1996, *77*, 3865.

(58) Kresse, G.; Joubert, D. *Phys. Rev. B* 1999, *59*, 1758.

(59) Kittel, C. *Introduction to Solid State Physics*, 6th ed.; Wiley: NY, 1986.

(60) Neugebauer, J.; Scheffler, M. *Phys. Rev. B* 1992, *46*, 16067.

(61) Monkhorst, H. J.; Pack, J. D. *Phys. Rev. B* 1976, *13*, 5188.

(62) Methfessel, M.; Paxton, A. T. *Phys. Rev. B* 1989, *40*, 3616.

(63) Ohta, T.; Kitajima, Y.; Stefan, P. M.; Shek Stefan, M. L.; Kosugi, N.; Kuroda, H. *J. Phys. Coll.* 1986, *C8*, 503.

(64) Heuer, D.; Müller, T.; Pfnür, H.; Kohler, U. *Surf. Sci. Lett.* 1993, *297*, L61.

(65) Alfonso, D. *Surf. Sci.* 2008, *602*, 2758.

(66) Galea, N. M.; Kadantsev, E. S.; Ziegler, T. *J. Phys. Chem. C* 2007, *111*, 14457.

(67) Kitajima, Y.; Yagi, S.; Yokoyama, T.; Imanishi, A.; Takemaka, S.; Ohta, T. *Surf. Sci.* 1994, *320*, L89.

(68) Lin, X.; Ramer, N. J.; Rappe, A. M.; Hass, K. C.; Schneider, W. F.; Truot, B. L. *J. Phys. Chem. B* 2001, *105*, 7739.

(69) Raghavachari, K. *J. Chem. Phys.* 1990, *93*, 5862.

(70) Rodriguez, J. A.; Hrbek, J.; Kuhn, M.; Jirsak, T.; Chatuverdi, S. *J. Chem. Phys.* 2000, *113*, 11284.

(71) Rodriguez, J. A.; Dvorak, J.; Jirsak, T.; Liu, G.; Hrbek, J.; Aray, Y.; Gonzalez, C. *J. Am. Chem. Soc.* 2003, *125*, 276.

(72) Alfonso, D. R. *Surf. Sci.* 2005, *596*, 229.

(73) Cotton, F. A.; Wilkinson, G. *Advance Inorganic Chemistry*; Wiley, New York, 1988.

(74) Dennert, R.; Sokolowski, M.; Pfnür, H. *Surf. Sci.* 1992, *271*, 1.

(75) Henkelman, G.; Arnaldson, A.; Jonsson, H. *Comp. Mat. Sci* 2006, *36*, 254.

(76) Sanville, E.; Kenny, S. D.; Smith, R.; Henkelman, G. *J. Comput. Chem.* 2007, *28*, 899.

(77) Wu, Y. K.; Mitchell, K. A. K. *Can. J. Chem.* 1989, *67*, 1975.

"Table of Contents" Graphic